Phys. Status Solidi B **251**, No. 1, 53–80 (2014) / **DOI** 10.1002/pssb.201350136

physica status solidi b
www.pss-b.com
basic solid state physics

Part of Topical Section on
Computational Thermodynamics

Feature Article

Lambda transitions in materials science: Recent advances in CALPHAD and first-principles modelling

Fritz Körmann[*,1], Abed Al Hasan Breidi[2], Sergei L. Dudarev[3], Nathalie Dupin[4], Gautam Ghosh[5], Tilmann Hickel[1], Pavel Korzhavyi[6], Jorge A. Muñoz[7], and Ikuo Ohnuma[8]

[1] Max-Planck-Institut für Eisenforschung GmbH, 40237 Düsseldorf, Germany
[2] Interdisciplinary Centre for Advanced Materials Simulation, Ruhr-Universität Bochum, 44780 Bochum, Germany
[3] EURATOM/CCFE Fusion Association, Culham Centre for Fusion Energy, Oxfordshire OX14 3DB, UK
[4] Calcul Thermodynamique, 63670 Orcet, France
[5] Department of Materials Science and Engineering, Northwestern University, 2220 Campus Drive, Evanston, IL 60208-3108, USA
[6] Department of Materials Science and Engineering, KTH Royal Institute of Technology, Brinellvägen 23, 100 44 Stockholm, Sweden
[7] California Institute of Technology, W. M. Keck Laboratory 138-78, Pasadena, California 91125, USA
[8] Department of Materials Science, Tohoku University, Aoba-yama 6-6-02, Sendai 980-8579, Japan

Received 16 August 2013, revised 5 November 2013, accepted 8 November 2013
Published online 20 December 2013

Keywords CALPHAD, first principles, lambda transitions, magnetism, thermodynamic modelling

[*] Corresponding author: e-mail koermann@mpie.de, Phone: +49 (0)211 6792 930, Fax: +49 (0)211 6792 465

This paper provides a comprehensive overview of state-of-the-art computational techniques to thermodynamically model magnetic and chemical order–disorder transitions. Recent advances as well as limitations of various approaches to these so-called lambda transitions are examined in detail, focussing on CALPHAD models and first-principles methods based on density functional theory (DFT). On the one hand empirical implementations – based on the Inden–Hillert–Jarl formalism – are investigated, including a detailed interpretation of the relevant parameters, physical limiting cases and potential extensions. In addition, Bragg–Williams-based approaches as well as cluster-variation methods of chemical order–disorder transitions are discussed. On the other hand, it is shown how magnetic contributions can be introduced based on various microscopic model Hamiltonians (Hubbard model, Heisenberg model and beyond) in combination with DFT-computed parameters. As a result of the investigation we were able to indicate similarities between the treatment of chemical and magnetic degrees of freedom as well as the treatment within the CALPHAD and DFT approaches. Potential synergy effects resulting from this overlap have been derived and alternative approaches have been suggested, in order to improve future thermodynamic modelling of lambda transitions.

1 Introduction The classification of second order phase transitions as 'λ transitions' in a variety of materials is motivated by the special shape of the graph of heat capacity as a function of temperature in these materials. The terminology was first introduced in the context of the superfluid transition in helium by Keesom and Keesom [1]. Nowadays it is also used for the description of transitions in many other material classes, such as superconductors, magnetic systems and alloys. In the field of computational thermodynamics of materials, two second-order transitions that exhibit such a lambda-shaped heat capacity curve are particularly important: a transition from a magnetically ordered to a paramagnetic configuration (a prominent example is the case of Fe illustrated in Fig. 1) and a chemical order–disorder transition in alloys. Both of them significantly influence the thermodynamic properties and phase stabilities in a large variety of elemental materials (unaries) and compounds and are therefore highly relevant for materials science. At the same time, the magnetic transitions have particularly attracted the attention of computational scientists, due to the challenges in physical modelling and mathematical analysis that they pose.

As a part of a series of manuscripts initiated during the 2013 Ringberg Unary Workshop (RUW2013), the present

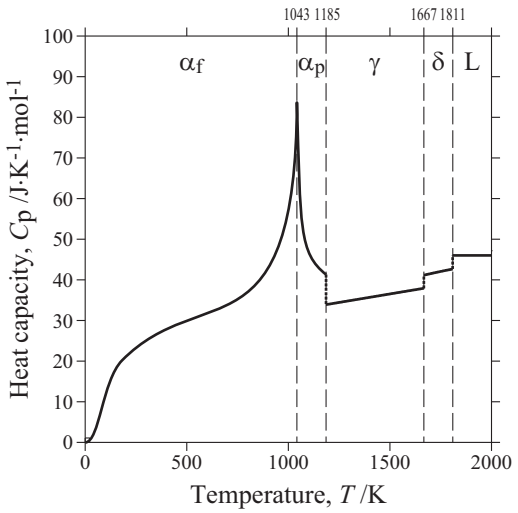

Figure 1 The heat capacity of iron calculated using CALPHAD and parameters proposed in Ref. [2].

paper is dedicated to the current state-of-the-art CALPHAD (calculation of phase diagrams) and first-principles (or in latin: *ab initio*) models for those Gibbs energy contributions that give rise to these two types of lambda transitions. In a previous paper by de Fontaine et al. [3], which was the result of a similar workshop held about 20 years ago, the authors outlined the methodology for treating the magnetic transitions available at that time. Since then, many new concepts have been developed. In addition – accompanied by the dramatic growth of the available computational resources – first-principles calculations, in particular represented by density-functional theory, have become highly successful and established theoretical tools in materials science.

The research topics and questions arising within the CALPHAD and first-principles communities have naturally overlapped more and more in recent years and consequently both communities have increasingly grown together. Eventually this resulted in greater interest in linking the concepts underlying both approaches. In this manuscript we therefore provide not only an overview of the state-of-the-art methods related to CALPHAD and first-principles modelling of lambda transitions, but we also discuss potential connections, overlaps and similarities between both concepts. For this purpose, a comprehensive introduction into those CALPHAD as well as finite temperature DFT simulations is given, which focuses on various aspects of magnetic and atomic lambda-transitions, and in particular on the correspondence between phenomenological and first-principles modelling techniques.

Within the CALPHAD approach, magnetic order–disorder transitions and magnetic Gibbs energy contributions are described by the formalisms that was first introduced by Inden [4]. This approach, although based entirely on empirical assumptions, turned out to be suitable for fitting the experimental heat capacity data for a large range of magnetic materials. Various aspects and recent developments of the model are discussed in Section 2. One particular concern is to provide a compact view of the first-principles theoretical methods for studying magnetic contributions. Introducing microscopic model Hamiltonians, such as the Hubbard or the Heisenberg model, is a commonly used approach in studies of electronic correlations and magnetic excitations. These models are suited to describe certain fashions of magnetism (itinerant or localized magnetism) and have their individual strengths and shortcomings. Section 3 is dedicated to providing a compact introduction into these models and how they are often used in combination with first-principles methods. A long-term objective here is to develop a physically well founded, yet practical and analytically tractable magnetic model, which could be implemented in the current CALPHAD approach. To this extend, the current Inden-based model is discussed in detail with respect to its known physical limitations. Possible alternative models are discussed in Section 4.

Atomic order–disorder transitions are commonly described by Bragg–Williams-based approaches, which usually have shortcomings with respect to short-range order effects. The latter could be improved by using more sophisticated approaches such as the cluster variation method. Here both methods are described in Section 5, and it is shown how they are used in either CALPHAD or first-principles based approaches.

The delicate interplay between atomic and magnetic degrees of freedom is discussed in Section 6. The coupling can result in complex interaction contributions. For instance, chemical ordering can influence the magnetic critical temperature, whereas magnetic ordering can have a substantial impact on the crystal elastic properties. A way of incorporating this effect into the CALPHAD approach is discussed and its application is illustrated with the examples Fe–Al and Fe–Ni alloys. Finally, the balance of atomic and magnetic contributions and their impact on phase stabilities is discussed for the phase transition sequence in pure Fe.

2 CALPHAD approaches for magnetic transitions

When separately discussing the magnetic contribution to the Gibbs energy, one implicitly performs an adiabatic approximation. This is based on the fact that in the solid state the magnetic (as well as electronic and vibrational) degrees of freedom are typically much faster than the configurational (diffusion-controlled) degrees of freedom in alloys and compounds. Thanks to this separation on the time scale, an alloy phase may be considered completely equilibrated with respect to the fast (including magnetic) degrees of freedom at a given temperature. This procedure uniquely defines the non-configurational part of the free energy as a single-valued function of temperature at every point in the domain of atomic configurations.

One should always be aware that further separation of the non-configurational energy into its electronic, magnetic and vibrational parts is not robust. Although it is justified for several materials and in some limiting cases (such as at $T \rightarrow 0$), the separation of these contributions in terms of the relevant time scales is generally not obvious. Instead the electronic, magnetic and vibrational excitations in a solid

are interdependent in real materials, and their contributions to the heat capacity are hard to separate in experiments and derived thermodynamic models, especially at high temperatures. First principles simulations have the advantage that one can switch off and on these degrees of freedom one-by-one, thereby evaluating the individual thermodynamic contributions. However, one must keep in mind also that here the total effect is generally not additive due to mutual interactions among the different excitations.

Within thermodynamic models such as CALPHAD, the procedures adopted to single out the magnetic contribution to the heat capacity [5] are based upon the experimental fact that the heat capacity of a single-phase solid (which does not undergo any ordering transition) is a smooth and continuous function of temperature. In such cases the non-configurational heat capacity is comprised of vibrational and electronic contributions. Consequently, any singularity in the heat capacity is completely ascribed to a magnetic ordering. It is then added on top of the regular temperature dependence due to the vibrational and electronic excitations in the solid. For the sake of convenience, the latter contributions to all thermodynamic functions are assumed to be continuous across the magnetic ordering temperature. As a result of this procedure, the singular (magnetic) contribution is chosen to vanish far away from the transition temperature, i.e. in the $T \to 0$ and $T \to \infty$ limits. By construction, magnetic excitations such as fluctuations of the magnitude of magnetic moments (the corresponding heat capacity contribution is an increasing function of temperature) are not part of the magnetic term, but are effectively included in the electronic contribution.

Preferably, the representation of magnetization should be a simple closed expression formulated using a minimum number of model parameters. The expression should nevertheless be flexible enough to represent the singular magnetic contribution to thermodynamic properties of any elemental solid, as well as of every magnetically ordered phase in a multicomponent alloy at any point in the domain of the concentration variables and atomic order parameter variables.

The realization of these requirements in CALPHAD is mainly based on the 1976 model of magnetism proposed by Inden [4], which provides an 'empirical and approximate analytical' formula for the magnetic contribution to the heat capacity C_p^{mag}. Although a number of modifications, e.g. those described in Refs. [4, 6, 7], have been suggested since then, the overall character of the approach has not changed: the formulas are still constructed such that the experimental data are fitted in the above mentioned spirit, but not such that any physical laws are fulfilled.

It is worth mentioning that the solid above and below the critical magnetic ordering temperature T_{C} should, strictly speaking, be considered as two different phases. In particularly important cases (such as Fe, Co and Ni) the high- and low-temperature magnetic phases are, however, crystallographically very similar and one continues to describe them as a single phase with a lambda-shaped anomaly in the temperature dependence. Nevertheless, the magnetic model of magnetism below and above T_{C} is different, due to a change in magnetic character. The former region is dominated by a long-range order (LRO) of the magnetic degrees of freedom. The temperature region above the critical temperature is, in most cases, not solely characterized by a random distribution of directions for the local moments, but short-range order (SRO) plays a decisive role. The asymmetry in the lambda-shape of the heat capacity next to the critical temperature makes different descriptions necessary. The material-specific parameters considered are related to physical quantities and therefore typically not subject to a fit to experiment (Section 2.2). The approach performs surprisingly well for most magnetic materials that have so far been considered by Inden and others, but the lack of physical foundation limits the predictive power of magnetism in CALPHAD.

2.1 Traditional CALPHAD approaches to magnetism Despite the different nature of magnetism below and above T_{C}, the approach of Inden [4] for its description is characterized by a very similar structure for the LRO and SRO models. Motivated by the study of ln–ln plots of various elements, the suggested analytic expression for the magnetic contribution to the heat capacity as a function of reduced temperature $\tau = T/T_{\mathrm{C}}$ is given by:

$$C_p^{\mathrm{LRO}} = K^{\mathrm{LRO}} \cdot R \cdot \ln \frac{1 + \tau^{m_{\mathrm{LRO}}}}{1 - \tau^{m_{\mathrm{LRO}}}} \quad \text{for } \tau < 1, \tag{1}$$

$$C_p^{\mathrm{SRO}} = K^{\mathrm{SRO}} \cdot R \cdot \ln \frac{1 + \tau^{m_{\mathrm{SRO}}}}{1 - \tau^{m_{\mathrm{SRO}}}} \quad \text{for } \tau > 1. \tag{2}$$

Here, R is the gas constant. The only difference in the structure of Eqs. (1) and (2) is the choice of the exponent, for which Inden suggested $m_{\mathrm{LRO}} = 3$ and $m_{\mathrm{SRO}} = -5$.

While this equation looks consistent, the empirical character is contained in the temperature-independent prefactors, given by

$$K^{\mathrm{SRO}} = \frac{0.784 \cdot f \cdot S^{\mathrm{mag}}/R}{0.5979 - 0.2114 f}, \tag{3}$$

$$K^{\mathrm{LRO}} = \frac{S^{\mathrm{mag}}/R - 0.493 K^{\mathrm{SRO}}}{0.822}. \tag{4}$$

They contain two further parameters, f and S^{mag}, which both have a physical origin: f is defined as the ratio between the magnetic enthalpy due to SRO and LRO and given by the following expression:

$$f = \frac{\Delta H^{\mathrm{SRO}}(\infty)}{\Delta H^{\mathrm{SRO}}(\infty) + \Delta H^{\mathrm{LRO}}(T_{\mathrm{C}})}, \tag{5}$$

where ΔH is the enthalpy change as obtained from an integration of the heat capacities in Eqs. (1) and (2) over the temperature interval in the SRO or LRO regime, respectively. The second quantity S^{mag} denotes the magnetic entropy

Table 1 Magnetic constants as used in the Inden approach [4] to magnetism.

	Fe	Co	Ni
T_C	1043 K	1380 K	631 K
β	2.22	1.7	0.6
f	0.4	0.28	0.28

as it is obtained significantly above the magnetic ordering temperature $T \gg T_C$:

$$S^{\text{mag}} = R \ln(\beta + 1), \tag{6}$$

where $\beta = \langle\mu\rangle/\mu_B$, μ_B is the Bohr magneton (i.e. the magnetic dipole moment of a single electron), and $\langle\mu\rangle$ the ensemble averaged magnetic moment.

Together, the Inden approach contains three physically motivated parameters: (i) the critical temperature T_C, (ii) the magnetic moment β and (iii) the SRO versus LRO ratio f. These parameters are summarized in Table 1 for the most investigated unary ferromagnets Fe, Co and Ni. The coincidence that the value of f is the same for Co and Ni led to the conclusion that the value $f = 0.28$ should be used for all fcc ferromagnets. Similarly the value $f = 0.4$ for Fe has been generalized as being the correct choice for all bcc ferromagnets.

The approach of Inden [4] turned out to be numerically too complicated for the efficient calculation of phase diagrams. Hillert and Jarl [6] suggested a modification: they kept the same set of parameters and the same basic structure of the expression for the heat capacity, but used an approximate power series expansion of Eqs. (1) and (2),

$$C_p^{\text{x}} = K^{\text{x}} R \left(\tau^{m_{\text{x}}} + \frac{1}{3}\tau^{3m_{\text{x}}} + \frac{1}{5}\tau^{5m_{\text{x}}} \right), \tag{7}$$

where x = SRO/LRO. In this expression the values of $m_{\text{LRO}} = 3$ and $m_{\text{SRO}} = -5$ remained unchanged. The prefactors are provided as $K^{\text{SRO}} = 0.918 \ln(\beta + 1)$ and $K^{\text{LRO}} = 0.6417 \ln(\beta + 1)$. The decisive advantage of such an expression is the fact that it does not yield a mathematical divergence at the critical temperature T_C.

Chen and Sundman [2] have proposed to extend the series expansion of Hillert and Jarl by another term and to work with

$$C_p^{\text{x}} = K^{\text{x}} R \left(\tau^{m_{\text{x}}} + \frac{1}{3}\tau^{3m_{\text{x}}} + \frac{1}{5}\tau^{5m_{\text{x}}} + \frac{1}{7}\tau^{7m_{\text{x}}} \right). \tag{8}$$

In addition, they modified the parameter m_{SRO} to the value -7. The resulting shape of the heat capacity in iron is shown in Fig. 1.

The suggestion of Hillert and Jarl [6] is currently the most commonly used description of the magnetism of unaries within CALPHAD databases. It is also used for binaries and more complex alloys.

2.2 Interpretation of parameters The nature of the magnetic CALPHAD models introduced in the previous section are order–disorder transitions, considering the thermodynamic contributions due to the orientational degrees of freedom of the atomic magnetic moments. This is similar in spirit to the Heisenberg picture of localized moment magnetism (see Section 3.2). Indeed, many magnetically ordered systems exhibit features (like the lambda-shaped heat capacity peak) that are similar to the prediction of the Heisenberg model, although systems where the atomic magnetic moments are strictly localized are extremely rare. Free energy contributions from fluctuations of the magnetic moments in magnitude (due to Stoner excitations in itinerant magnets or due to low-spin to high-spin transitions in atoms exhibiting valence fluctuations) are not accounted by the magnetic term in CALPHAD, but are effectively included in the remaining free energy terms (ascribed to electronic or vibrational excitations).

By construction, the magnetic contributions to energy (enthalpy) and entropy in the CALPHAD model are finite at all temperatures, similar to those in the (quantum) Heisenberg model. It is therefore convenient to use their limiting values corresponding to $T \to \infty$,

$$H_{\text{max}} = \int_0^\infty C_P^{\text{mag}}(T)\,\mathrm{d}T \sim k_B T_C \tag{9}$$

and

$$S_{\text{max}}^{\text{mag}} = \int_0^\infty \frac{C_P^{\text{mag}}(T)}{T}\,\mathrm{d}T \sim k_B \ln(\beta + 1), \tag{10}$$

as measures of the maximum magnetic enthalpy and entropy, respectively, of an alloy phase. Here $C_P^{\text{mag}}(T)$ is the magnetic part of the heat capacity, which is also a function of the concentration and order parameter variables (see Section 2.3).

It follows from Eq. (9) that the T_C parameter in the CALPHAD magnetic model is not only the temperature of the heat capacity peak, it also normalizes the enthalpy change due to the magnetic order–disorder transition in the alloy phase (with the proportionality constant of the order of unity). Similarly, the β parameter normalizes the entropy due to the magnetic disordering transition. This entropy can be interpreted as the maximum degree of orientational disorder of localized magnetic moments in the paramagnetic state (β being the effective paramagnetic moment) only for systems exhibiting a Heisenberg-like behaviour. For itinerant magnets this interpretation is inaccurate. However, the formalism can be generally applied as long as it provides a good description of the thermodynamic contributions due to the lambda-peak of heat capacity.

2.3 Composition dependence of magnetic ordering We started the considerations on magnetism by discussing the splitting up of free energy contributions related to different degrees of freedom. The traditional CALPHAD approaches to magnetism as outlined in Section 2.1 together

with the employed separation can be justified as long as the whole non-configurational free energy is modelled accurately. Modifications, however, turned out to be required if one tries to describe the composition dependencies of the regular 'non-magnetic' (vibrational plus electronic) and of the singular 'magnetic' parts of the free energy in a thermodynamically consistent way. Due to the relevant consequences for magnetic modelling, we are discussing this aspect next.

The standard representation of the composition dependence in CALPHAD employs an interpolation in terms of smooth Redlich–Kister (R–K) polynomials. For the regular non-magnetic part of the free energy this works fine. For the singular part, composition dependencies of the model parameters, namely, the critical temperature T_C and the Bohr magnetic moment β (see Section 2.2), has been used. [1] However, the composition dependence of T_C values in a multicomponent single phase (so-called magnetic phase diagram) can be complex and difficult to represent in terms of a smooth function. Different composition regions may exhibit different types of magnetic ordering: ferromagnetic, FM; antiferromagnetic, AFM or more complicated structures. At some compositions there may be several magnetic ordering transitions as a function of temperature, while at some others there may be no magnetic ordering at all.

Some alloy systems of practical importance have been successfully treated with a single composition dependence of the critical (Curie) temperature in the ferromagnetic ordering region. In the AFM ordering region, where a mean-field formula for the FM Curie temperature would give a negative value, the same curve (multiplied by a factor of -1 for bcc or $-1/3$ for fcc structure) has been used to describe the composition dependence of the Néel temperature [8]. Indeed, in cases where the magnetic ordering is dominated by the nearest-neighbour exchange interaction such an approach can work, but it can also be expected to have problems in systems with more complicated exchange interactions. It was therefore recommended by Xiong et al. to represent the critical temperatures corresponding to different types of magnetic ordering (FM or AFM) separately, using different R–K polynomial functions of concentration variables [9]. The composition dependencies of model parameters used in the standard and improved magnetic models are presented in Fig. 2.

The composition dependence β is another difficult issue. One idea, originating from a correlation between saturation magnetization and Curie temperature of ferromagnets, was to impose an additional condition of proportionality between β and T_C. Thus, in a random binary alloy exhibiting FM on the one side and AFM ordering on the other, the Curie temperature and magnetic moment would both go through zero at a certain composition c_0. At first sight this constrained model looks thermodynamically consistent as the magnetic contribution vanishes automatically in the $T \to 0$ limit (to satisfy the Nernst theorem). However, at the composition where the T_C goes through zero, the magnetic free energy contribution would be exactly zero at all temperatures, while at any other composition away from c_0 the magnetic contribution would be negative. Clearly, this 'anomaly' would grow bigger and bigger with temperature, opening up an artificial miscibility gap centred at c_0 (see Fig. 3).

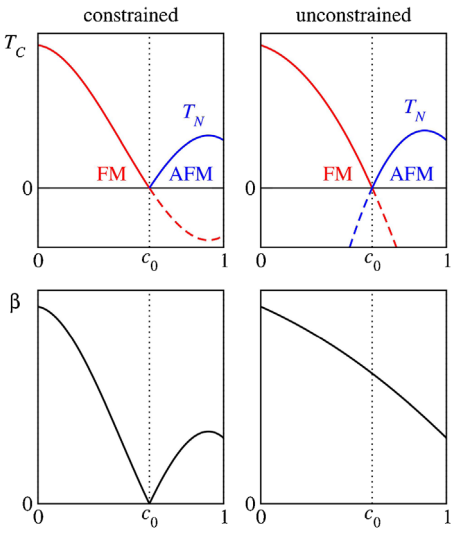

Figure 2 Upper panels: Composition dependencies of the Curie temperature T_C and Néel temperature T_N predicted by a constrained (left) and unconstrained (right) CALPHAD magnetic model for a hypothetical binary alloy system exhibiting a crossover between ferromagnetic (FM) and antiferromagnetic (AFM) ordering at concentration c_0. Lower panels: Corresponding composition dependence of the Bohr magnetic moment β.

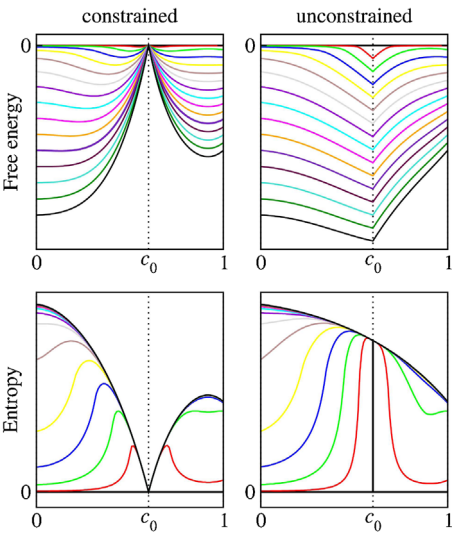

Figure 3 Composition dependencies of magnetic free energy (top panels) and entropy (bottom panels) given by the standard (constrained, left) and improved (unconstrained, right) magnetic models. The lines are plotted for temperatures in the range from 0 K to $3 \cdot T_C(0)$ with a temperature step of $0.2 \cdot T_C(0)$.

[1] In addition to composition dependence, the dependence of T_C and β on the order parameter values must be described for ordered solid solution phases, which is modelled in CALPHAD using the Compound Energy Formalism (see Section 5).

The origin of this behaviour is the artificial constraint on the composition dependence of the β parameter. Removing this constraint was suggested [9] in order to enable proper modelling of a quite general alloy case where the transition from FM to AFM ordering at concentration c_0 occurs due to the sign change of the (dominant) magnetic exchange interaction, while the magnitudes of atomic magnetic moments behave smoothly as functions of composition. As the magnetic moments are related to the maximum magnetic entropy (see Section 2.2), the free energy in this unconstrained model will also remain smooth in the high-temperature limit due to the dominant $-TS$ term (see Figs. 2 and 3).

The magnetic contribution in the unconstrained model also vanishes as $T \to 0$, but the magnetic entropy for alloys near c_0 remains finite down to low temperatures (and down to 0 K at c_0). This 'zero-point entropy' is physically meaningful: the atoms possess magnetic moments which cannot order because of too weak or frustrated magnetic interactions in the alloys close to c_0. In real alloys such magnetic disorder is often found to form a partial magnetic order, i.e. to freeze into a spin-glass state. Complex magnetic behaviour can also be exhibited by systems in which magnetism disappears as a function of composition or pressure. In this cases once again, the critical temperature(s) and magnetic moments do not have to disappear at the same point [10]. It is clear that the CALPHAD magnetic model, even in its unconstrained version, is too crude to give a detailed description of such complex magnetic transitions.

2.4 Experimental studies and limitations of the CALPHAD approach The modelling of magnetic properties and of composition dependencies of ordering temperatures strongly depends on the availability of reliable experimental data. In particular, the measurement of heat capacities provides very valuable information. For unaries like Fe, Co and Ni, a large number of such experimental data is available (see, e.g. Refs. [4, 11]). As a side product they allow us to determine T_C by identifying the corresponding position of the (lambda-shaped) peak in the heat capacity. In the case of Fe shown in Fig. 1, for example, this yields a T_C value of 1043 K.

One of the drawbacks of current magnetic models within CALPHAD is their inability to actually predict a magnetic structure of a phase/alloy. Instead, a certain magnetic model – currently being limited to FM, AFM and the SRO regime – is chosen to describe the free energy of the system knowing its magnetic structure. Typical experimental techniques used to establish the magnetic structure are neutron diffraction, Mössbauer spectroscopy, magnetometry, etc. At the same time, it is highly desirable to complement experimental results with first-principles calculations (see Section 3).

The experimental situation becomes particularly challenging for phases that are thermodynamically not stable. With respect to magnetic properties, γ-iron at room temperature is a prominent example. Experimentally γ-iron is stabilized mostly in combination with fcc Cu, e.g. by annealing Fe alloys in Cu (see, e.g. [12, 13]) or by epitaxial growth of thin Fe layers on Cu(001) (see, e.g. [14]). About 50 years ago, susceptibility and neutron diffraction studies [15, 16] indicated an AFM character. In later studies on ultrathin films, a non-monotonous variation of the magnetization was found, which was assigned to the formation of a helical spin-wave (characterized by $q_{\text{exp}} = 2p/a(0.127, 0, 1)$) [13]. The non-collinear spin-spiral state was also later confirmed by first-principles calculations, see, e.g. Ref. [17] and references therein.

Another experimental approach to study the magnetic properties of γ-iron is through of Fe-based alloys. Both γ-Fe–Mn and γ-Fe–Cr–Ni alloys have been widely used as model systems to study the AFM order at low temperatures, and to measure the transition temperature (Curie or Néel) as well as sublattice magnetic moments. AFM ordering in γ-Fe–Mn was established in 1956. Sedov [18] showed that in the composition range of 13–44 at% Mn, the susceptibility is temperature independent above the Néel temperature, implying that localized moments are absent in the PM state. In their seminal work, Ishikawa and co-workers [19–23] established a magnetic phase diagram of γ-Fe–Mn in the entire composition range. They showed that the AFM order of γ-Fe–Mn is stabilized by a different mechanism than the end-members, γ-Fe and γ-Mn.

While a two-state (high-spin vs. low-spin) model for austenitic Fe–Ni alloys has been discussed in the literature [24, 25], Mössbauer spectroscopy of Fe-28 to 30 at% Ni alloys show the co-existence of FM and AFM phases [26, 27], implying exchange anisotropy. A deconvolution of the Mössbauer data allows to determine the amounts of FM and AFM phases. To date, however, no attempt has been made to quantify coexistent magnetic phases within the CALPHAD approach.

An established method to measure Curie temperatures (as well as the order–disorder transition temperatures discussed below) is differential scanning calorimeter (DSC). Here, second order (lambda-shaped) transitions can be recognized as sharp valleys upon heating and maxima upon cooling in the DSC curves. As an example, we discuss in the following paragraph some interesting results for the Fe–Co–Si system, for which DSC measurements shown in Fig. 4 [28] provide information about magnetic as well as chemical ordering.

Since T_C for Fe–25Co–8Si (at%) alloy is higher than its A2/B2 transition temperature, the magnetic transition temperature corresponds to the disordered structure and the A2/B2 transition temperature to the FM state. The opposite is observed in Fe–12.5Co–12Si (at%), where T_C corresponds to the B2 ordered structure and the A2/B2 transition temperature to the PM state. The vertical section phase diagram between Fe–50Co and Fe–16Si alloys in Fig. 5 summarizes these findings. Here, the paramagnetic A2/B2 boundary was extrapolated to the fictitious paramagnetic Fe–50Co alloy at 270 °C. The actual A2/B2 transition temperature of

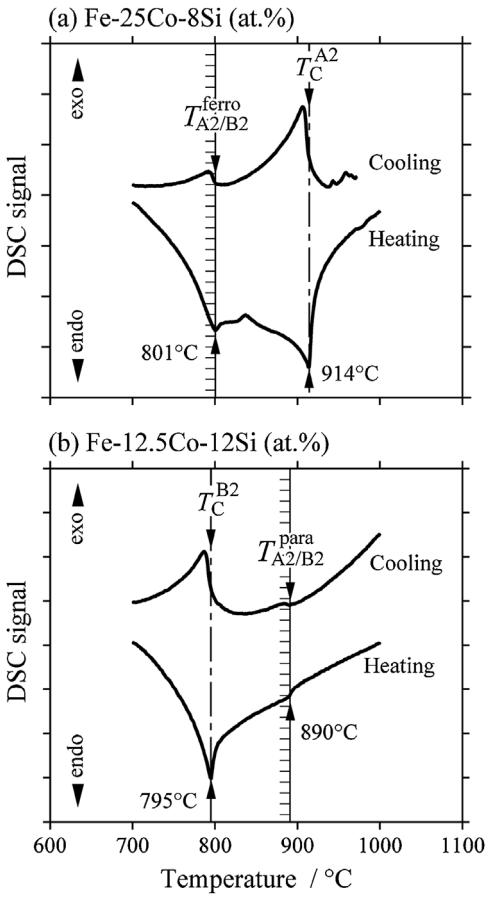

Figure 4 DSC curves of the magnetic and chemical ordering of Fe–Co–Si alloys.

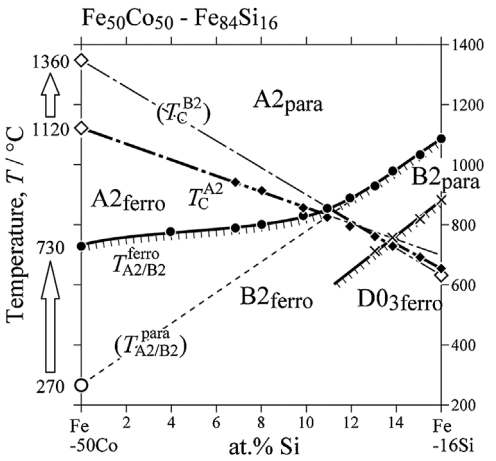

Figure 5 Vertical section phase diagram of bcc phases in the Fe–Co–Si system.

ferromagnetic Fe–50Co alloy is 730 °C, significantly higher. It is evident that a strong interaction between the magnetic and the chemical ordering is relevant in this material system, which motives corresponding studies in Section 6. In the same manner, the Curie temperatures of the metastable A2 structure (1120 °C) and of the fictitious B2 structure (1360 °C) of Fe–50Co can be estimated experimentally.

Another interesting aspect is the effect of pressure (P) on T_C, which has been in detail studied in three alloy systems: Fe–Ni, Fe–Pd and Fe–Pt by Wayne and Bartel [29]. Plotting the dependence they surprisingly found a single descending curve fitting roughly the empirical relation $\partial T_C/\partial P = -(1600/T_C)\mathrm{K}^2/\mathrm{kbar}$. Nakamura et al. [30] showed that Mn-containing invar alloys also exhibited a rather similar behaviour where both $\partial \ln T_C/\partial P$ and the high field susceptibility χ_o varied in a parallel manner as Mn content was varied. Based on their findings, the authors concluded that the magnetoelastic coupling constant is insensitive on the chemical composition. In their study of pressure dependence of the magnetic moment in Fe–Al alloys, Noakes et al. [31] found a rather complex behaviour of the magnetization as a function Al-concentration. These and other studies indicate the challenges related to pressure effects on (magnetic) phase transitions, which are currently almost completely ignored in CALPHAD simulations. The effect of pressure is inherently complex due to the effect of volume strain on T_C *and* magnetic moment, and also due to associated magnetic phase transition (from FM to AFM), if any. We will not address these issues any further in this paper, but would like to refer to Ref. [32], where more details on the impact of pressure and strain on magnetic properties can be found.

3 *Ab initio* description of magnetism at finite temperatures

Having discussed the current (empirical) way of CALPHAD modelling of magnetic lambda-transitions, we now turn to the corresponding description from first principles. A *rigorous* first-principles simulation requires the solution of the many-body Schrödinger equation, containing the full Coulomb interaction between electrons and nuclei, which is of course not feasible. The Kohn–Sham formalism of density functional theory (DFT) is typically insufficient to capture the strong exchange-correlation effects underlying magnetic excitations. Instead of the Kohn–Sham Hamiltonian, therefore, other model Hamiltonians are introduced, which serve as simplified microscopic models to describe various magnetic excitations. A connection with conventional *ab initio* methods is established through a suitable choice of model parameters, which are determined by DFT calculations.

3.1 Model Hamiltonians

Model quantum-mechanical Hamiltonians provide a fundamental insight into how the localized ionic magnetic moments form and interact, showing that the origin of magnetism is associated with effects of electron–electron interaction. The idea of using model Hamiltonians to describe interaction between electrons

occupying localized atomic orbitals was pioneered by Anderson [33] and Hubbard [34]. The Anderson Hamiltonian

$$\hat{H} = \sum_{\mathbf{k},\sigma} \epsilon_{\mathbf{k}} \hat{n}_{\mathbf{k}\sigma} + E_0(\hat{n}_{d\uparrow} + \hat{n}_{d\downarrow}) + U\hat{n}_{d\uparrow}\hat{n}_{d\downarrow} + \sum_{\mathbf{k},\sigma} V_{d\mathbf{k}} \left(\hat{c}^{\dagger}_{\mathbf{k}\sigma}\hat{c}_{d\sigma} + \hat{c}^{\dagger}_{d\sigma}\hat{c}_{\mathbf{k}\sigma}\right) \quad (11)$$

describes a localized orbital d (occupied according to $\hat{n}_{d\sigma} = \hat{c}^{\dagger}_{d\sigma}\hat{c}_{d\sigma}$) exchanging electrons with the surrounding electronic liquid via the exchange term $V_{d\mathbf{k}}$. $c^{\dagger}_{\mathbf{k}\sigma}$ and $\hat{c}_{\mathbf{k}\sigma}$ denote the usual destruction and creation operators. In the electronic liquid, the non-interacting single-particle electron states ($\hat{n}_{\mathbf{k}\sigma} = \hat{c}^{\dagger}_{\mathbf{k}\sigma}\hat{c}_{\mathbf{k}\sigma}$ with wave vector $\mathbf{k}$) are characterized by the dispersion relation $\epsilon_{\mathbf{k}}$. U is the energy of Coulomb repulsion between two electrons with opposite spins $\sigma = \uparrow, \downarrow$ occupying the localized orbital, and E_0 is the unperturbed energy of the latter. Hubbard [34] constructed a broadly similar model, assuming that the localized orbitals form an infinite lattice, and replaced the electronic liquid term in Eq. (11) by a tight-binding inter-site electron hopping model. The Hubbard Hamiltonian has the form

$$\hat{H} = \sum_{i,j} t_{ij}\hat{c}^{\dagger}_{i\sigma}\hat{c}_{j\sigma} + U\sum_{i} \hat{n}_{i\uparrow}\hat{n}_{i\downarrow}, \quad (12)$$

where t_{ij} is a matrix of (spin-independent) tight-binding elements describing quantum hops of electrons between the localized orbitals centred on lattice sites i and j, and where the U-term has exactly the same meaning as the U-term of the Anderson Hamiltonian (11). The only difference between the Hubbard and the Anderson Hamiltonians is that in the Hubbard case the localized orbitals form a lattice whereas the Anderson Hamiltonian describes an isolated orbital interacting with its environment. The fundamental connection between the two models has been highlighted by recent developments in the mean-field theory treatments of the Hubbard (and Hubbard-like) Hamiltonians [35] in which the energy spectrum of a lattice Hubbard Hamiltonian is found by mapping it onto an Anderson model.

A fundamental drawback associated with both Hamiltonians (11) and (12) is that they describe interaction between electrons assuming that the electrons occupy localized orbitals of s-type. In other words, the Hamiltonians assume that the localized orbitals are non-degenerate and that they have no angular character. It has long been recognized in the literature on atomic spectroscopy [36, 37] that an atomic Hamiltonian describing interacting p-electrons must contain two independent parameters (i.e. for p-electrons it is not sufficient to specify only the magnitude of the U term). Similarly, a d-electron Hamiltonian must contain three independent parameters. The matter remained a subject of debate until very recently, with some authors effectively asserting the validity of the Hubbard Hamiltonian for the p- and d-electrons [38], with other authors treating either the full $(2l+1)^4$-element matrices describing the on-site electron–electron interactions [39] or simplifying it down to a tractable form while losing some of the symmetry properties [40–42]. For example, in a recent tight-binding treatment of magnetic FeCr alloys [43], the model Hamiltonian describing both the inter-site electron hopping and the on-site electron–electron interactions for the case of a degenerate d-band was taken in the form

$$\hat{H} = \sum_{i,j,\, i\neq j} \sum_{m,m',\sigma} t_{im,jm'}\hat{c}^{\dagger}_{im\sigma}\hat{c}_{jm'\sigma} + \sum_{i,m,\sigma} \epsilon_i \hat{c}^{\dagger}_{im\sigma}\hat{c}_{im\sigma} + \sum_{i} \left[\frac{U_i}{2} \sum_{m,m',\sigma} \hat{n}_{im,\sigma}\hat{n}_{im',-\sigma} + \frac{U_i - J_i}{2} \sum_{m,m',\sigma} \hat{n}_{im,\sigma}\hat{n}_{im',\sigma}(1-\delta_{mm'}) \right], \quad (13)$$

where indices m and m' refer to atomic orbitals, and the parameter U_i describes repulsion between electrons with anti-parallel spins occupying the same lattice site. The strength of repulsion is reduced by J_i if the spins of electrons are parallel. By re-arranging terms in the above Hamiltonian (13), it can be transformed, exactly, into the Stoner Hamiltonian [43]

$$\hat{H} = \sum_{i,j,\, i\neq j} \sum_{m,m',\sigma} t_{im,jm'}\hat{c}^{\dagger}_{im\sigma}\hat{c}_{jm'\sigma} + \sum_{i} \epsilon_i \hat{N}_i + \frac{1}{2}\sum_{i} \left(U_i - \frac{J_i}{2}\right)\left(\hat{N}_i^2 - \hat{N}_i\right) - \frac{1}{4}\sum_{i} J_i \hat{M}_i^2, \quad (14)$$

where $\hat{N}_{i,\sigma} = \sum_m \hat{n}_{im,\sigma}$ is the total, summed over all the orbitals m, number of electrons with spin σ on site i, and the operators $\hat{N}_i = \hat{N}_{i\uparrow} + \hat{N}_{i\downarrow}$ and $\hat{M}_i = \hat{N}_{i\uparrow} - \hat{N}_{i\downarrow}$ refer to the total number of electrons on a lattice site, and to the total magnetic moment (in the electrons per atom units) on a site. The above derivation shows that parameter I of the Stoner model is identical to parameter J characterising intra-atomic exchange interaction. In the literature the Stoner parameter is sometimes identified with the Hubbard U, see for example [44], which is incorrect. The origin of the confusion lies in the incorrect application of the Hubbard Hamiltonian, formulated for s-electrons, to the d-electron case.

A fully covariant Hamiltonian describing hopping and on-site interaction between p- and d-electrons has recently been derived by Coury et al. [45]. In comparison with the Stoner Hamiltonian (14), the Coury Hamiltonian is invariant with respect to rotations of the Cartesian axes and also with respect to the unitary transformation of the basis on-site orbitals. In the Coury Hamiltonian, like in the Stoner Hamiltonian (14), the term proportional to the square of the magnetic moment operator has negative sign. This favours the formation of non-vanishing local magnetic moment due to the total energy minimization argument.

3.2 Heisenberg-based approaches The Heisenberg Hamiltonian describes the low energy part of the spectrum of electronic excitations in a magnetic material. The occurrence of the low-energy excitations, described by an approximate Heisenberg or a Heisenberg-like Hamiltonian, is a well-known signature of electron correlations [46]. Magnetic electron correlations are described by a term, quadratic in the operator of magnetic moment, of the Stoner Hamiltonian (14). There are many ways of deriving the Heisenberg model Hamiltonian from the more microscopic Hamiltonians describing interacting electrons, one of the most common ones involves taking the large U limit of the Hubbard model (12). In this limit the effective Hamiltonian for the low energy part of the spectrum of electronic excitations has the form [38]

$$\hat{H} = -\sum_{i,j} J_{ij}\hat{\boldsymbol{S}}_i \cdot \hat{\boldsymbol{S}}_j, \tag{15}$$

where $\hat{\boldsymbol{S}}_i$ is the vector operator of the total spin associated with site i, and $J_{ij} = t_{ij}^2/U$. Energy taken in the form Eq. (15), where $\boldsymbol{S}$ is treated as a classical vector variable, is often *postulated* as a mathematical expression to which results of *ab initio* calculations are fitted, for example such an approach is used for deriving the Heisenberg exchange parameters J_{ij} from density functional theory [47]. To map *ab initio* data onto the Heisenberg model, a second-order perturbation theory approach is applied where the inter-site Heisenberg parameters are identified with the suitably chosen second derivatives of the total energy of a magnetic system with respect to the relative orientations of the moment unit vectors of neighbouring ions. An alternative approach to the evaluation of J_{ij} in real space is the so-called spin-spiral approach, which provides an elegant way of computing the Fourier-transformed parameters $J_{\mathbf{q}}$ in $\boldsymbol{q}$-space [48]. Both methods are complementary and have their individual strengths and shortcomings (see e.g. Ref. [49] where the two methods are compared). Nowadays, Eq. (15) is extensively used in combination with DFT calculations to extract the effective magnetic exchange interactions [49–56].

The quantum version of the Heisenberg model (15) was originally proposed by Heisenberg [57] and Dirac [58] to mimic the quantum magnetism of localized electrons. In the Heisenberg–Dirac picture $\hat{\boldsymbol{S}}_i$ are treated as operators of atomic spin or the total angular moment, coupled through the inter-site exchange parameters J_{ij}. As discussed above, within a classical interpretation of the model, the $\boldsymbol{S}_i$ are treated as continuous three-dimensional vectors, whereas in the quantum case they are represented by operators obeying the standard commutator rules and having discrete eigenvalues. In the classical picture, valid in the limit where the number of discrete eigenstates $2S + 1 \gg 1$, quantum fluctuations of moments are neglected. Operators of the on-site total angular moment $\hat{\boldsymbol{S}}$ and the associated local magnetic moment $\hat{\boldsymbol{M}}$ are related via

$$\hat{\boldsymbol{M}} = g_J \mu_B \hat{\boldsymbol{S}}, \tag{16}$$

where the Landé-factor is $g_J \approx 2$. In many applications employing Eq. (15), it is assumed that electronic configurations of individual ions do not change and the moments do not vary in terms of their magnitude. In this case the S^2 scaling factor can be absorbed into the J-parameters, defining effective $\tilde{J} = J^{\mathrm{cl}}S^2$ in the classical or $\tilde{J}^{\mathrm{qm}} = J^{\mathrm{qm}}S(S+1)$ in the quantum case. [2]

For practical implementation within the CALPHAD formalism, a mathematically closed analytic expression of the solution of Eq. (15) would be required. Unfortunately, it is generally not possible to derive the complete and exact spectrum of its eigenstates in an explicit analytical form. The simplest approximate solution for the magnetization of the Heisenberg model is the Weiss mean-field (MF) approach (compare also BWG approach in Section 5.1 for chemical disorder). Using Green's function techniques [62], improved analytical solutions like the random-phase approximation (RPA) [49, 53, 54] become accessible.

The common approach to solve the *classical* Heisenberg model numerically is a classical Monte Carlo (cMC) technique, which can be used to evaluate the energy, the entropy, and the Gibbs energy of the model for an arbitrary set of J_{ij} parameters [50–53]. The quantum-mechanical counterpart of this technique, the Quantum Monte Carlo (QMC) approach, [63, 64] has limited applicability due to the so-called (negative) sign problem [65, 66]. For realistic material systems, which are characterized by oscillating and long-ranged positive as well as negative magnetic exchange integrals [49], the QMC solution of the quantum Heisenberg model is generally not feasible.

Applied to materials like bcc Fe, the analytical RPA approach as well as the cMC simulations provide both reliable predictions for selected properties such as the magnetic critical temperature T_C [49, 51, 52, 55, 56, 67, 68]. Körmann et al. [56, 68, 69] have recently investigated the advantages and limitations of these methods, if used for the derivation of temperature dependent properties like the specific heat of bcc Fe (see Fig. 6). The analytical RPA (solid purple line in Fig. 6) approach typically provides an excellent treatment of the thermodynamic properties in the LRO regime below T_C, much better than MF (dashed purple line in Fig. 6). This

[2] One has to note that there is no well defined rule for how to absorb S into J within the quantum model [59], since the on-site moments in fact vary as a function of their length, exhibiting what is known as longitudinal fluctuations of moments [52, 60]. Another way of renormalising the exchange parameters in the transverse-fluctuations-only limit of the quantum Heisenberg model would be to adopt $\tilde{J}^{\mathrm{qm}} = S^2 J^{\mathrm{qm}}$, similar to how it is introduced in the classical formulation of the model. This does not however account for the quantum nature of the spins. In contrast to this, the definition involving the $S(S+1)$ factor is rooted in the quantum nature of the spin operators, i.e. it is based on the eigenvalue relation of angular momentum operators $\boldsymbol{S}^2|S\rangle = S(S+1)|S\rangle$. Such a definition of the effective exchange coefficients is useful in particular when results of the classical and quantum solution are compared [56, 59], since the thermodynamic quantities approximately scale in the quantum case as $S(S+1)$. Note that T_C within the quantum case does not strictly vary as $T_C(S) \sim J^{\mathrm{qm}}S(S+1)$ as was recently shown using the high temperature series expansion [61].

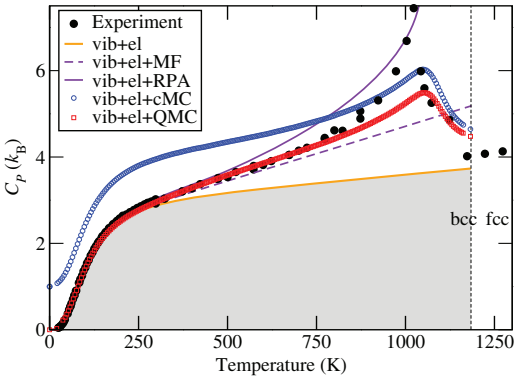

Figure 6 Specific heat capacity of bcc Fe and comparison of different analytic and numerical treatments of the Heisenberg model Eq. (15) [70].

shortcoming is also found for MF treatments for both, magnetic (Fig. 6) and chemical order–disorder approaches (BWG in Section 5.1). A better description of the SRO is obtained by cMC simulations, again in agreement with the corresponding treatment of chemical disorder (see Section 5).

One drawback of cMC is its failure at lower temperatures in the LRO regime due to the neglect of spin quantization [56, 69]. In addition, cMC (and also RPA) exhibit deficiencies in predicting the net magnetization curves $M(T)$ [68]. It has been shown that these limitations can be overcome by employing semi-empirical rescaling approaches [56, 70] that rescale the existing cMC data using an analytic function. Such a function can be derived for model systems, where both, the classical and quantum mechanical, results are available. A careful analysis of a large set of such data revealed an universal relation between classical and quantum results, independent of the crystal structure (bcc, fcc, etc.), type of magnetism (FM or AFM), and interaction range. Based on this insight, a universal analytic function could be formulated [56], which allows one to transform classical results into approximate quantum ones. The approach has been successfully applied to bcc Fe (red squares in Fig. 6) [56].

Another alternative is to map the (typically) long-ranged Heisenberg model onto an effective nearest-neighbour model, which is usually free of magnetic frustration.[3] Here the effective nearest-neighbour exchange parameter is fitted to an existing experimental or theoretical critical temperature. Such an approach has been successfully applied to pure elements such as Fe, Co and Ni [69] as well as to more complex magnetic structures such as Fe_3C [71]. The latter is a good example where finite-temperature first-principles data may help improve the quality of CALPHAD models (see Section 4.1).

Still the main issue impeding a practical implementation of the Heisenberg-model based treatment within the CALPHAD approach is that there is still no analytical expression solving Eq. (15) reasonably well over the entire temperature range, both in the LRO and the SRO regime. A potential alternative model based on a Landau-type expansion for the magnetic free energy will be discussed in Section 4.3.

3.3 Extensions of the Heisenberg model How well does the classical Heisenberg Hamiltonian describe how the total energy varies as a function of directions of magnetic moments? This question was posed by Drautz and Fähnle [72], and has recently been explored in considerable detail by Singer et al. [73] who investigated how the total energy of bcc and fcc iron, computed using density functional theory, varies on a hyper-surface spanned by the directions of atomic magnetic moments. They concluded that *ab initio* calculations provide sufficient evidence that the energy of a magnetic material is described by a more complex function of directions of magnetic moments than the sum of binary scalar products of magnetic moments as assumed within the Heisenberg Hamiltonian Eq. (15).

Another, almost obvious, limitation of the Heisenberg model Eq. (15) is that it assumes that magnetic moments, while having variable orientation, remain constant as functions of their magnitude $M_i = |\boldsymbol{M}_i|$ (here instead of spins $\boldsymbol{S}_i$ we use magnetic moment $\boldsymbol{M}_i$ as independent variables). This aspect of magnetic excitations, associated with longitudinal (i.e. length) fluctuations of magnetic moments, has been investigated by Ruban et al. [52], and by Ma and Dudarev [60]. Ruban et al. [52] mapped the energies computed *ab initio* to a classical Heisenberg model, in which the intersite exchange parameters were treated as functions of the magnitude of magnetic moments. Limitations of the Heisenberg model, associated with the itinerant character of electrons in 3d transition metals, have also been discussed in detail by Capellmann [74]. Ma and Dudarev [60] explored the dynamics of longitudinal magnetic fluctuations using a Heisenberg–Landau model, first proposed by Lavrentiev et al. [75, 76], in which the energy of ions treated as functions of the orientation and magnitude of magnetic moments has the form

$$E(\{\boldsymbol{M}_i\}) = -\sum_{i,j} J_{ij}\boldsymbol{M}_i \cdot \boldsymbol{M}_j + \sum_i \left(A_i \boldsymbol{M}_i^2 + B_i \boldsymbol{M}_i^4 + C_i \boldsymbol{M}_i^6\right). \quad (17)$$

In the Heisenberg–Landau model the moments are treated as three-dimensional vector variables, where in principle their magnitude is not constrained from above or below, and where an attempt to vary the magnitude of a moment is controlled by the second, Landau, term in Eq. (17). Such a term is not included in the standard Heisenberg model (15) which therefore does not treat longitudinal magnetic fluctuations. A surprising aspect of the classical Heisenberg–Landau model, Eq. (17), is that it is more efficient computationally than the original, seemingly simpler, classical Heisenberg model (15). In Monte Carlo [76] or

[3] A counter-example is a magnetically frustrated nearest-neighbour antiferromagnetic three-dimensional fcc lattice.

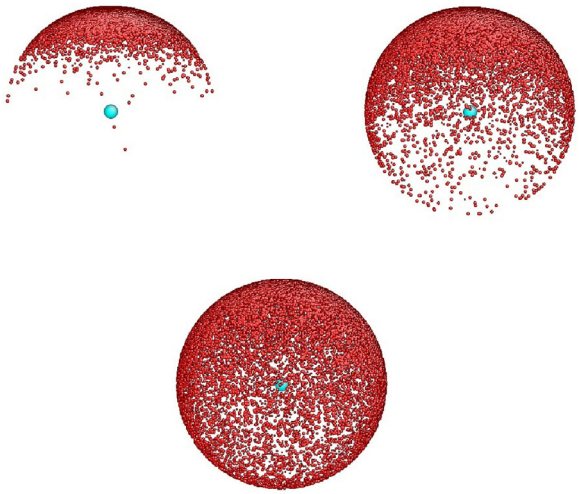

Figure 7 Distribution of directions of magnetic moments on a unit sphere found using spin-lattice dynamics simulations for pure Fe at 300, 800 and 1100 K. Note that at temperatures below the Curie temperature the dominant orientation of the moments is 'up', whereas at 1100 K, above the Curie temperature, the directions of moments are homogeneously distributed over the entire surface of the unit sphere.

spin dynamics [60] simulations (Fig. 7) it proves easier to explore configurations defined in three-dimensional space spanned by vectors $\boldsymbol{M}_i$ than to analyse the statistics, or dynamic evolution, of moments defined on a hyper-surface spanned by moments varying only as a function of their direction $|\boldsymbol{M}_1|, |\boldsymbol{M}_2|, \ldots, |\boldsymbol{M}_N| = \text{const}$. The Heisenberg–Landau Hamiltonian has proved effective in the treatment of finite temperature magnetic properties as well as magnetism-driven structural phase transitions in Fe–Cr [76] and Fe–Rh [77] alloys.

An interesting point related to the treatment of the Heisenberg model concerns the dynamic time-dependent aspect of evolution of magnetic states of the system. Statistical treatment of phase diagrams assumes ergodicity, which implies equivalence between the time-dependent and time-independent approaches to sampling configurations spanned by a magnetic system. The dynamic evolution of a magnetic system described by a Heisenberg Hamiltonian was extensively explored by Ma et al. [60, 78–81]. Of particular interest in view of the statistical interpretation of dynamic simulations is the notion of temperature of evolving interacting magnetic moments [80]

$$k_{\mathrm{B}}T = \frac{\left\langle \sum_i [\boldsymbol{M}_i(t) \times \boldsymbol{H}_i(t)]^2 \right\rangle_t}{2\left\langle \sum_i \boldsymbol{M}_i(t)\boldsymbol{H}_i(t) \right\rangle_t}, \tag{18}$$

where $\boldsymbol{H}_i(t) = -\partial E(\{\boldsymbol{M}_i(t)\})/\partial \boldsymbol{M}_i(t)$ is the time-dependent effective exchange field acting on moment $\boldsymbol{M}_i(t)$, and both the numerator and denominator are statistically averaged over the ergodically evolving magnetic system. Equation (18) shows that the temperature of magnetic moments can be positive or negative, depending on the sign of the average scalar product of moments and exchange fields. The temperature of magnetic moments is zero if every magnetic moment is collinear with the exchange field acting on it [82].

4 Improved description of magnetism for CALPHAD

The ultimate goal for an improved description of magnetism within CALPHAD would be a replacement of the empirical IHJ formula (see Section 2.1) for the magnetic Gibbs energy by an approach that is physically motivated. As already indicated at the beginning of Section 2, such a selective modification is not straightforward, since the magnetic part in the established thermodynamic models does typically not describe the *full* contribution due to the magnetic degrees of freedom. Mainly the (lambda shaped) singularity in the heat capacity is ascribed to magnetism, while the smooth and continuous parts of the non-configurational Gibbs energy (which still include implicit magnetic effects) are captured by terms associated with electronic and vibrational contributions.

A strategy to keep within CALPHAD the established description for non-magnetic degrees of freedom untouched, but to replace *only* the magnetic description by a new model will therefore most likely not work. Instead, any change in the magnetic model can only be performed in a parallel effort with corresponding (physcially motivated) modifications for the other contributions. Possible strategies in this direction will be discussed in Sections 4.2 and 4.3. Before coming to this point, however, we would first like to elucidate the chances of using *ab initio* based simulations of magnetism discussed in Section 3 for an improved CALPHAD modelling.

4.1 Using *ab initio* like experiments

In contrast to CALPHAD approaches, *ab initio* simulations have the advantage that they are free of empirical assumptions and fitting parameters. Since all physical results are derived from the fundamentals of quantum mechanics, the direct usage of *ab initio* energies for the modelling of thermodynamic functions is of course an attractive option. However, there are two drawbacks of such an approach:

(i) Despite its quantum-mechanical origin, it is well known that the most established *ab initio* method, namely density functional theory (DFT), is by no means exact. While many of the numerical approximations can be systematically improved, the treatment of the exchange-correlation functional (within LDA, GGA or other approaches) remains an uncontrolled approximation. The relative differences in energies (already at $T = 0$) obtained with different exchange-correlation (xc) functionals and correspondingly the inaccuracies of the DFT data are often larger than typical experimental error bars.

(ii) It has been shown in the previous section that in the case of magnetic excitations, even *ab initio* based approaches are not free of empirical assumptions. Instead, model Hamiltonians that can only partly cover the complexity of nature, are extensively employed. The reliability of the models for a

real system at hand can often only indirectly be checked and this again requires a comparison with experiment.

Nevertheless, it has been demonstrated by various examples that electronic [11], vibrational [11], defect [83] or pressure [32] effects can indeed be identified by sufficiently accurate *ab initio* calculations. As mentioned above, however, the way magnetism is currently incorporated into the CALPHAD formalism makes a separate treatment of magnetic free energies and the identification of the IHJ free energy contributions with a result of an *ab initio* calculation as obtained in Section 3 hardly possible.

Until this problem is rigorously resolved, *ab initio* based methods should be employed differently in order to improve the simulation of magnetic materials in CALPHAD. Instead of using *ab initio* energies and entropies as parts of the thermodynamic CALPHAD modelling, it seems to be much more promising to exchange those data between the methods, which would otherwise be taken from experiment, i.e. to consider *ab initio* methods as 'virtual matter experiments' [84]. In the following we provide some examples of such an approach. In particular we focus on the *ab initio*-derived mean magnetic moments of two alloys, on the derivation of critical temperatures from first-principles, and on the application to the specific heat capacity of Fe_3C.

The magnetic moment corresponds to the Bohr magneton number β and is therefore one of the three parameters in the IHJ model. It determines according to Eq. (6) the maximum magnetic entropy, but governs also the intensity of the lambda-peak in the C_p curve at the transition temperature. Experimentally, it is not trivial to measure the local on-site magnetic moments, as it requires sophisticated technics such as neutron diffraction, Mösbauer spectroscopy or XMCD. In contrast to this, the magnetization (i.e. the mean magnetic moments) can be measured routinely by standard magnetometry methods.

Ab initio methods have proven to be particularly powerful, if chemical trends over a larger range of chemical compositions are considered. Within the CALPHAD approach, such composition dependencies for β as well as for the transition temperature T_C are fitted to the Redlich–Kister polynomials (see also Section 2.3). In the absence of experimental data for such a fit, it is possible to compute both local (or onsite) and mean magnetic moments using first-principles methods.

There are several methods to compute the composition dependence of mean magnetic moments in chemically random alloys. The most common ones are the supercell method, usually in combination with the concept of special quasi random structures [95], and the coherent potential approximation (CPA) (a recent review is given in Ref. [96]), where the alloy is simulated by an effective potential. Application of both approaches can be found, e.g. in Refs. [97, 98]. The CPA approach is in general numerically much less demanding, but typically does not yield quantitatively more accurate results than supercell approaches. Alternatively, the mean magnetic moments can also be determined by the cluster expansion (CE) technique, which we will show in the following.

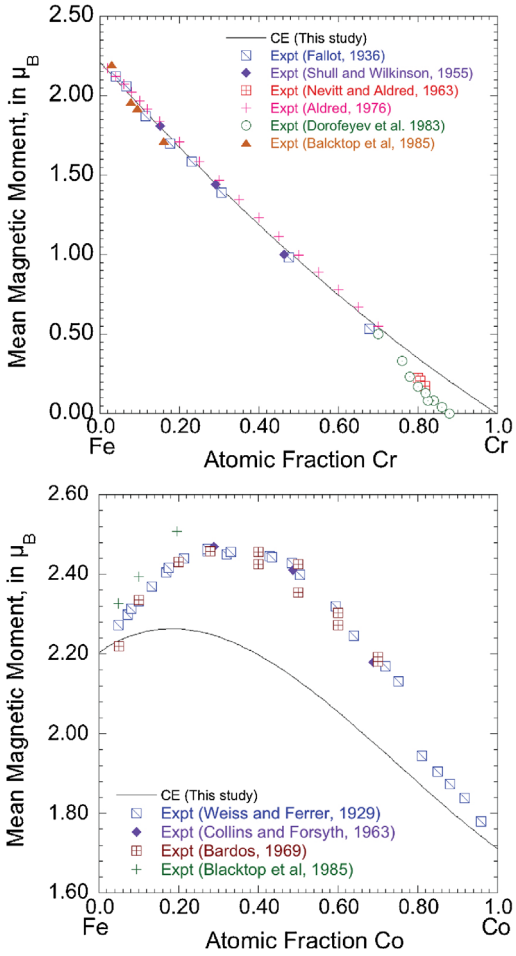

Figure 8 A comparison of mean magnetic moment (β) in bcc solid solution computed using cluster expansion (CE) technique shown as solid line [85] and experimental data: (upper panel) Fe–Cr [86–91], (lower panel) Fe–Co [91–94] alloys.

In the upper panel of Fig. 8 a theoretical result for the composition dependence of β in a bcc Fe–Cr solid solutions is compared with experimental data [85, 99]. Here, the solid line is based on *ab initio* energies [4] of ordered phases and a subsequent cluster expansion of the magnetic moments defines the mean magnetic moment in a disordered bcc solid solution. Thirty-seven ordered structures were used for the CE of bcc-Fe–Cr alloys [85], and total energies were calculated assuming each ordered structure to be ferromagnetic.

The experimental data are obtained with neutron diffraction [87] and magnetometry [86, 88–91]. Noticeable deviations only occur for Cr contents of more than 70 %, where the onset of anti-ferromagnetism is observed in experiment, while AFM configurations are not considered in the present CE approach. In addition, the lower panel in Fig. 8 demonstrates for the Fe–Co example that the composition dependence of β does not need to show a linear behaviour

[4] The VASP code has been employed [100] using projector-augmented plane waves [101], GGA-PW91 [102] and a cutoff-energy of 410 eV.

as in the Fe–Cr case. In the CE of bcc Fe–Co alloys we have used 33 ordered structures [85]. As seen in Fig. 8b, the mean magnetic moment initially increases as Co is added to Fe reaching a maximum around 30 at% Co [92–94, 91] and decreases for larger Co contents. In this case there is only a qualitative, but not a quantitative agreement of the CE results with the experiments, indicating also the limitations of the method.

For both alloys, similar results were obtained by the CPA approach by Olsson et al. [97] for Fe–Cr and by Richter and Eschrig [103] for Fe–Co.

Note that conventional CE and SQS approaches are limited to magnetically collinear ordered structures, which fails if non-collinear configurations dominate the physical properties as shown, e.g. for Fe–Ni alloys by van Schilfgaarde et al. [104].

The second experimental parameter, which enters the IHJ model, is the Curie temperature. As explained earlier, this quantity is not directly accessible to *ab initio* calculations, but it requires model Hamiltonians for the thermodynamic evaluation. Heisenberg-like Hamiltonians (Section 3.2) and their extensions (Section 3.3) are most often used for this purpose. The models themselves can be solved via classical Monte Carlo simulations [50–53] or within many-body theory [49, 53, 54]. In both cases, the obtained Curie temperatures are known to provide reasonable agreement with experiment. These methods are nowadays commonly employed and provide successful predictions even for complex systems such as, e.g. diluted magnetic semiconductors [67], Fe–Co-alloys [51], or Heusler alloys [105], to name a few of them. An alternative are the pioneering works by Kübler et al. employing the spin-fluctuation theory (see Ref. [106] and references therein, as well as [107–109] for recent applications). We note that effects which are usually neglected in computational schemes for T_C-predictions, such as lattice expansion, electronic excitations and structural defects, can be of significant importance as has been recently shown by Alling et al. for complex alloys ($Ni_{1-x}Cu_xMnSb$) [110].

Beyond these approaches, the recently achieved dramatic progress in the *ab initio* simulation of finite temperature properties provides also the possibility for a new class of 'virtual matter experiments'. Instead of calculating physically motived parameters for thermodynamic models such as that of IHJ, the whole thermodynamics can be captured by *ab initio* calculations. What worked already nicely for several non-magnetic materials (see also Ref. [11]) can nowadays also be performed for magnetic systems.

One example is the recent assessment by Hallstedt et al. [111] for cementite (Fe_3C), one of the most common and important precipitate phases in steels. Despite its fundamental importance, the experimental variety of data for the heat capacity shown in Fig. 9 (black symbols) makes the situation inconclusive. In particular, in the paramagnetic region above the Curie temperature, even qualitatively different trends are observed in experiment. This implies also difficulties to set up a proper magnetic model, to reliably treat this phase in CALPHAD approaches. Therefore, established databases for the Fe–C system like the one of Gustafson [112] consider the heat capacity of Fe_3C as a constant.

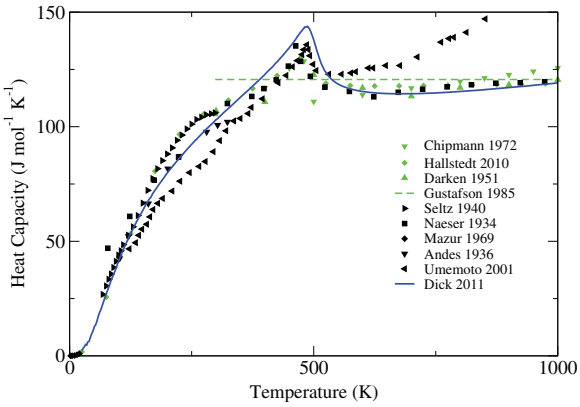

Figure 9 Specific heat capacity of Fe_3C. *Ab initio* derived data by Dick et al. [71] in comparison with available experimental data and CALPHAD assessments. The theoretical *ab initio* data deserved as an input for the most recent assessment by Hallstedt et al. [111].

Combining state-of-the-art theoretical techniques as the discussed QMC method (Section 3.2) with highly accurate DFT calculations, an *ab initio* based prediction of the thermodynamic properties of Fe_3C became recently possible [71] (see blue line in Fig. 9). It is reasonable to assume that the accuracy of this DFT calculation is much higher than the scatter in the experimental data. Based on the insights provided by the theoretical calculations, Hallstedt et al. reassessed the data which yielded an improved description of the Fe–Mn–C phase diagram in particular for lower temperatures [111]. We believe that this strategy will in future be of increasing importance for various magnetic materials, where experimental data are scare or inconclusive.

4.2 Exploiting exact limits The identification and exploitation of exact analytical relations for magnetic properties is a perfect starting point for the development of new thermodynamic models that should be physically motivated. As already pointed out in Section 3, an analytic function describing the various aspects of magnetism within one single unified theory most likely does not exist. However, there are limiting cases, which allow the derivation of exact analytical expressions, which should be universally correct for the majority of magnetic materials. In the following we will concentrate on two properties of the magnetic heat capacity: (a) the analytic low temperature dependence due to the collective excitation of spin waves and (b) the critical exponents close to the magnetic phase transition.

4.2.1 Low temperature limit It is well known that the magnetization of a ferromagnetic material is only saturated at $T = 0$, whereas gap-less excitations dominate the thermodynamic properties already at very low temperatures. These collective excitations of local magnetic moments, which are called spinwaves or magnons, dominate the magnetic response of the material and hence the heat capacity

C_p^{mag} in the limit $T \to 0$. Moreover, it can be rigorously proven that the spin wave excitations with wave vector $\mathbf{q}$ and energy dispersion $\omega_{\mathbf{q}}$ are eigenstates of the quantum-mechanical Heisenberg model (see Section 3.2), which makes their analytical description particularly easy.

At low temperatures the long-wave length behaviour of $\omega_{\mathbf{q}}$ is decisive. As shown by Bloch [113] one finds for a three-dimensional isotropic ferromagnet (FM) a quadratic dependence $\omega_{\mathbf{q}\to\mathbf{0}}^{\mathrm{FM}} \sim q^2$, which eventually results in a $T^{3/2}$ power law for C_p^{FM} (similar to the famous Bloch law for the magnetization of a ferromagnet):

$$C_p^{\mathrm{FM}}(T \ll T_{\mathrm{C}}) \sim T^{3/2}. \tag{19}$$

It is very instructive to consider in addition the results for a three-dimensional antiferromagnet (AFM). In 1950 Kubo showed [114] that the spin waves of an antiferromagnet behave as $\omega_{\mathbf{q}\to\mathbf{0}}^{\mathrm{AFM}} \sim q$ (similar to phonons) and therefore the specific heat capacity follows a Debye-like behaviour

$$C_p^{\mathrm{AFM}}(T \ll T_{\mathrm{C}}) \sim T^3. \tag{20}$$

The different temperature dependencies expressed in Eqs. (19) and (20) already indicate the challenges for developing a general thermodynamic model for magnetic Gibbs energies, which ideally should cover both types of magnetism (FM and AFM) on the same footing.

The traditional CALPHAD approaches presented in Section 2.1 are designed to describe in particular the lambda-peak in the heat capacity rather then the limit $T \to 0$. Nevertheless, one can easily convince oneself that the dominating low-temperature term in the original Inden formula (Eq. 1) as well as in the simplification of Hillert and Jarl (see Eq. (7) is

$$C_p^{\mathrm{Inden}}(T \ll T_{\mathrm{C}}) \sim T^3, \tag{21}$$

which would correspond to the behaviour of an AFM, while the models were originally deduced from data on ferromagnets. We note that a T^3 power law is also included in the analytic Debye model employed for fitting the low temperature lattice contribution to the specific heat [11].

4.2.2 Critical temperature We now turn our attention to the opposite end of the magnetization curve, namely the behaviour very close to the phase transition temperature T_λ. This regime is characterized by critical exponents, which are for a general function $f(\theta)$ defined as

$$a \equiv \lim_{\theta\to 0} \frac{\log|f(\theta)]}{\log|\theta|}, \tag{22}$$

where $\theta = (T - T_\lambda)/T_\lambda$ is the reduced temperature, which is zero at the phase transition. The critical exponent describes the dominant power law behaviour $f(\theta) \sim \theta^a$ of the function f close to T_λ . The advantage for a thermodynamic modelling is the fact that the critical exponents are not material specific, but are identical for whole universality classes of materials.

Table 2 Critical exponent α obtained from experiment, the Heisenberg model, classical Landau theory and the Inden model.

experiment	Fe [115]	−0.10
	Ni [115]	−0.095(5)
	EuO [116]	−0.12(2)
	$Fe_xNi_{80-x}B_{19}Si$ (x = 10, 13, 16, 20) [117]	−0.114(5)
	$RbMnFe_3$ [118]	−0.11(1)
theory	3D Heisenberg model [119]	−0.1336(5)
	Landau theory [120]	0
	Inden model	0

For the magnetic specific heat capacity the critical exponent close to the transition temperature $T_\lambda = T_{\mathrm{C}}$ is called α, yielding to the expression

$$\lim_{T\to T_{\mathrm{C}}} C_p(T) \sim |T - T_{\mathrm{C}}|^{-\alpha}. \tag{23}$$

In principle, α and α' respectively for the LRO and SRO region can be distinguished, but in most models $\alpha = \alpha'$ has been found. In Table 2 some experimental and theoretical data for α are shown. The available experimental data are similar for ferro- and antiferromagnetic systems (e.g. Fe and EuO), underlying the universal character of the exponent. It is interesting to note that these values are very close to the critical exponent obtained for the 3D Heisenberg model, i.e. that the presented materials and the model fall into the same universality class. This might be interpreted as a further indication why Heisenberg-like models perform reasonably well for a large number of systems.

Evaluating Eq. (22) with the empirical equation for the Inden model, Eqs. (1) and (2), yields a vanishing critical exponent. The value is the same as for the (classical) Landau theory, where the zero is a consequence of its mean field nature. It is not completely clear, how relevant the deviation of the critical exponent from the experimental data really is for the performance of the thermodynamic model. On the one hand, the power-law behaviour (23) typically applies only in a very narrow temperature range around the critical temperature. In this context it should also be mentioned that the experimental estimation of critical exponents is rather difficult since even a small amount of impurities can have a dramatic impact as for instance recently pointed out by Kuz'min and Tishin [121].

On the other hand, scaling theories are meanwhile established in fields like magnetocalorics, in order to simulate the field dependence of magnetic properties [122] close to transition temperatures. These strategies employ critical exponents for the definition of universal equations of states (e.g. see Ref. [123]), which require only a few material specific data in order to subsequently model regimes that are not available or accessible experimentally. The generalization of these concepts to the thermodynamic modelling of phase diagrams seems to be a promising.

4.3 Alternative models The alternative magnetic model, envisaged at the beginning of this section, should not only be physically motivated, but also meet a number of further challenges. The exact limiting cases discussed in Section 4.2 are one possible criterion. For practical applicability, the model should in addition represent a fair compromise between accuracy, practicality and flexibility, but should also yield an analytical expression that can be implemented into codes.

In particular these practical aspects make the exploitation of the methods that where already successfully applied to bcc Fe (see Fig. 6 of Section 3.2) and other materials challenging. Even the introduced analytical approaches based on RPA [55, 68] do not provide a closed mathematical expression for the Gibbs energy, but require a self-consistent iteration. To overcome these problems, a promising alternative might be an analytic expression for the heat capacity, recently proposed by Kuz'min [124]. It is based on the classical Landau theory combined with a semi-empirical condition for the magnetization shape. Here we shortly summarize the main findings. A detailed derivation can be found in Refs. [124–126].

The starting point is an expression proposed by Ginzburg for the thermodynamic potential for a ferromagnet Φ, which is based on the more general form proposed by Landau [127]. The potential is expanded in even powers of the magnetization M as [5]:

$$\Phi = \Phi_0 + \frac{1}{2}AM^2 + \frac{1}{4}BM^4 + \frac{1}{6}CM^6 + \cdots, \tag{24}$$

where the coefficients $A, B, C, \ldots$ can explicitly depend on temperature or external parameters like pressure.

We introduce three assumptions, namely (i) Eq. (24) is truncated after the M^6 term, (ii) coefficients B and C are temperature independent and (iii) coefficient A is of the form

$$A = A_0 \frac{\tau^3 - 1}{1 + p\tau^{3/2}}. \tag{25}$$

where $\tau = T/T_C$, and A_0 and p are parameters [124]. Eq. (25) ensures that the equation of state is consistent with Bloch's $T^{3/2}$-law for the magnetization. It was shown that the parameter p can be expressed in terms of the ground state magnetization M_0, T_C and spin wave stiffness D and can therefore in principle be determined from first-principles calculations [125, 126].

Kuz'min finally presented the analytic expression for the specific heat as

$$C^{\mathrm{mag}} = -\frac{\tau}{T_C}\left[\Phi_0''(\tau) + \frac{M_0}{2}A''(\tau)\sigma^2 + \frac{M_0}{2}A(\tau)''\frac{\partial\sigma^2}{\partial\tau}\right], \tag{26}$$

where $\sigma = M/M_0$ is the reduced magnetization.

[5] For simplicity we consider here only isotropic cases with no external magnetic field. A more general derivation is given in Ref. [124].

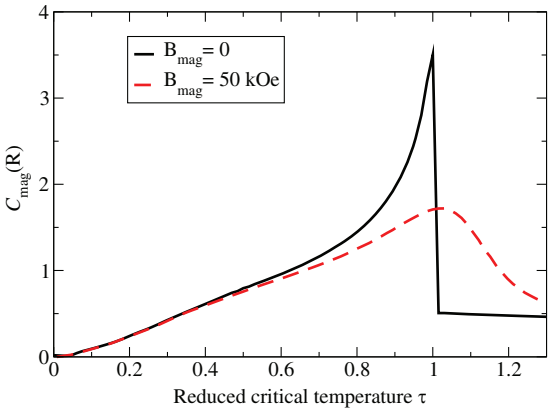

Figure 10 Application of Eq. (26) for Gd with and without external magnetic field. The data is taken from Ref. [124].

An application of Eq. (26) for Gd is shown in Fig. 10. These results nicely reveal the potential as well as the limitations of such a theory. One issue is the incorporation of short-range magnetic order above the critical temperature. As one can see for the case of vanishing magnetic field ($B_{\mathrm{mag}} = 0$), the underlying theory does not properly reproduce the experimentally observed decay of the magnetic entropy contribution in the SRO regime above T_C ($\tau > 1$). The reason behind is that the underlying Landau theory is in principle a mean field theory, which does not take into account magnetic SRO effects above the critical temperature (compare with purple lines in Fig. 6). The shortcoming goes along with the fact that the critical exponent of this approach does not come out correctly.

Nevertheless, the recent progress in developing such robust and physical magnetic models, justifies optimism in aiming at an analytic and 'as much physical as possible, but yet practical' theory for magnetic materials.

5 CALPHAD approaches to chemical order–disorder transitions As mentioned in the introduction, the chemical order/disorder transition is in addition to the magnetic transition another second-order phase transition that is critical for the thermodynamic modelling of many materials. Both phenomena share not only a similar lambda shape of the heat capacity. They also have in common that the transitions occur between an ordered state (i.e. with a long-range order) and a state that is disordered (where short-range order can still be present). In both cases the energy for the formation of bonds (between spins and atoms, respectively) determines the ordering tendency. Due to this conceptional similarity the desire to use similar method for simulating both transitions is not surprising.

Indeed, in the paper by de Fontaine et al. noted in Section 1, which has similar motivation as the present one, the authors did not see a need for describing the chemical order/disorder transitions separately, because they 'can also be mapped generally onto the Ising model' [3]. Also, Inden [4] in his seminal work on magnetic order/disorder

transitions in 1976 tested the applicability of the formalism given by Eqs. (1) and (2) to chemical ordering reactions. For the A2 $\leftrightarrow$ B2 transformation in CuZn, 'good agreement' between the empirically simulated and the measured C_p values next to the transition temperature was observed. In this case the values 0.2 and 0.3 were used for parameter f of the model (see Eq. 5, which highlights the fitting character of the approach based.

Despite these similarities, the physical origins of the two transitions are of course different. Correspondingly, several approaches have been developed that are specific to the chemical order/disorder transition. The most prominent examples are the Bragg–Williams based approaches and the cluster variation method, which will be discussed in this section. In Section 6, we will then comment on the coupling of magnetic and chemical order/disorder transitions.

5.1 Bragg–Williams based approaches The Bragg–Williams–Gorsky (BWG) approximation is a mean field approximation introduced independently by Bragg and Williams [128–130] and Gorsky [131] to describe chemical ordering. Within this theory an order parameter ξ is introduced, which depends via Boltzmann statistics on the energy V needed to move an atom from the position corresponding to the ordered structure to a wrong position with respect to such an ordering. The decisive assumption of BWG is that this energy V is itself proportional to the order parameter ξ and is vanishing in the completely disordered state. Therefore, V corresponds to the Weiss field introduced in mean-field theories of magnetism and similarly to the situation there (see, e.g. dashed violet line in Fig. 6), no correlations or short-range order are covered.

In the original treatment, the BWG approximation was dedicated to the description of the change of the degree of order with temperature for a given ordering structure. Examples are the change from an ordered $L1_2$-type structure to a fcc disordered (A1) phase, from a DO_3 to a B2 phase, or from a B2 to a bcc (A2) phase. Shockley [132] extended this approach for the treatment of the different atomic configurations on the fcc lattice observed in the Au–Cu system: the $L1_2$ phases based on Au_3Cu and $AuCu_3$ as well as the $L1_0$ phase AuCu. Rather than a single order parameter ξ, the occupations ξ_i of the four different simple cubic sublattices were used as parameters to express the energy and the configuration of the system. The phase diagram he calculated shows the stability of the four phases, including disorder (A1), the two $L1_2$ phases and the $L1_0$ ordered phase. According to this description the $Au_{50}Cu_{50}$ composition shows a complete disorder above a critical temperature, in disagreement with the experimental topology for the Au–Cu system.

The approach was further extended with its implementation in the compound energy formalism (CEF) for sublattices and applied to materials of industrial interest such as the Al-Ni system for the fcc case [133] and the Fe–Si system for the bcc case [134]. In this formalism the configurational entropy of ideal mixing is kept, but one introduces an energy of formation for each of the stoichiometric ordered configurations allowing more asymmetry than the use of a single pair interaction when considering binary systems. The formalism moreover allows the treatment of multicomponent cases [135].

5.2 Cluster variation method (CVM) The cluster variation method (CVM) is a generalization of the BWG approximation that was first proposed by Kikuchi [136] to treat cooperative phenomena in systems with ordering tendencies. As compared to the BWG approach, it has the advantage that not only long-range, but also short-range order can be described. Therefore, the shape of the heat capacity is obtained below as well as above the disordering temperature.

The CVM is based on a parameterization of the free energy (energy and entropy) by clusters of atoms (instead of pairwise interactions) that describe the local chemical configuration of the system. The energy is a linear function of the cluster concentration and the entropy is obtained from the equilibrium cluster distribution. The variational principle of statistical mechanics is then applied on the free energy functional by varying the configuration.

The inclusion of larger clusters generally gives more accurate results [137], but the original formulation of Kikuchi based on combinatorics makes it impractical to deal with very large clusters. Simplifications and reformulations such as those of Refs. [138–141] can make the problem more tractable. In practice, the number of considered clusters will be finite and relatively small, but this seems not to be a serious limitation as, e.g. the tetrahedron method [142] has been used to describe and correctly predict the behaviour of a large number of systems.

Some examples for treating chemical disorder with this method are discussed in the next subsections. Furthermore, the similar character of the order/disorder transitions also allows the application of the CVM to magnetic transitions. This can be demonstrated for the example of Gd (compare also Section 4.3), for which the IHJ model fails to capture the experimentally observed concave behaviour in the low temperature ($T \approx T_C/2$) part of the magnetic heat capacity. Figure 11 shows the result of the corresponding CVM simulation for a $S = 7/2$ Ising model in the tetrahedron approximation. Remarkable is the good agreement of the results with experiment in the LRO region, despite the limitation to nearest-neighbour interactions (similar to the QMC treatment of Fe in Section 3.2). However, for the approach seems to insufficient for SRO, where Monte Carlo simulations perform significantly better.

Another important application of the CVM formalism is to 'interpolate' the properties of random solid solutions of arbitrary compositions from values obtained for ordered structures, which are attainable by density functional theory. This is usually known as the cluster inversion technique [144]. In a random solid solution there is no correlation in the occupation of the atomic sites, so the correlation function depends only on the composition and the number of sites in the cluster. Sanchez et al. [145] showed that the set of clusters

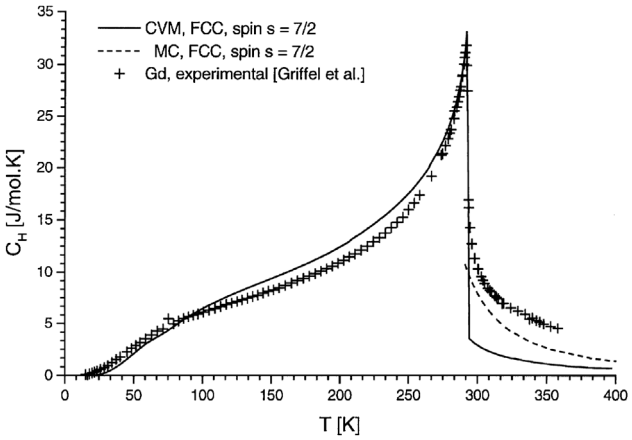

Figure 11 Application of the CVM in the tetrahedra approximation (solid line) to the magnetic part of the heat capacity of hcp Gd. The results are compared with Monte Carlo simulations (dashed line) and experiments (symbols, electronic and vibrational contributions substracted). The picture is taken from Ref. [143].

of all sizes are orthogonal to each other and form a basis, so any thermodynamic function can be mapped into this basis. In this case, the clusters are described by a scalar correlation function. This formalism is known as the cluster expansion (CE) method and is nowadays an established approach to treat disordered systems within DFT (see also Section 4.1) [95].

As discussed above on the example of the magnetic transition in Gd, MC simulations are usually the more accurate choice compared to CVM to account for SRO effects. Comparing CVM and MC simulations for chemical order–disorder transitions revealed, however, that the main topological effects due to the inclusion of SRO are reasonably well captured by the CVM approach (see, e.g. [146]). Furthermore, due to its analytic expressions, the CVM is in general computationally more efficient compared to MC simulations. For these reasons the limitations of BWG wrt. SRO contributions are mainly discussed in comparison with results obtained by the CVM method in the following.

5.3 Extensions of the CEF towards short-range order The BWG approximation and its CEF implementation are often criticized due to the topology fo the fcc coherent phase diagram obtained by Shockley. When comparing it with CVM results, this bad topology can be explained by the fact that the short-range order is not explicitely taken into account in mean field approximations. The thermodynamic behaviours of the ordered states calculated either by CEF or CVM are very close, in particular at low temperature, while the entropy of the disordered state is significantly overestimated by CEF.

However, the most advanced uses of the CEF consider reciprocal interactions allowing one to describe a prototype closer to CVM as discussed by Kusoffsky et al. [147]. In the case of an fcc structure with four sublattices the molar Gibbs energy of the phases is expressed as

$$G_m = \sum_{ijkl} y_i^{(1)}\, y_j^{(2)}\, y_k^{(3)}\, y_l^{(4)}\, G^{\circ}_{i:j:k:l} + \frac{1}{4}\sum_s \sum_i y_i^{(s)} \ln y_i^{(s)} + \sum_{s,r>s} y_A^{(s)}\, y_B^{(s)}\, y_A^{(r)}\, y_B^{(r)}\, L_{A,B:A,B}. \quad (27)$$

Here, the first term describes the mechanical mixing of the stoichiometric compounds, with $y_i^{(s)}$ being the site fraction of element i in sublattice (s). The second term provides the (ideal) configurational entropy on each sublattice. Most important is the third term that contains the reciprocal interaction parameters $L_{A,B:A,B}$ of element pairs A and B located in the two sublattices (s) and (r). This term represents a first approximation of the contribution to the Gibbs energy due to short range order.

Introducing an u that has the same value as the CVM pair bond energy, namely $-100R$, with R being the gas constant, the parameters are $G^{\circ}_{i:i:i:i} = 0$, $G^{\circ}_{i_3 j} = G^{\circ}_{ij_3} = 4u$ and $G^{\circ}_{i_2 j_2} = 6u$, $L_{A,B:A,B} = u$. Figure 12a compares the such obtained prototype fcc coherent phase diagram with that calculated with the CVM in the tetrahedra approximation. It turns out that the topology of the two phase diagrams are very close thanks to the stabilisation of the disordered stable introduced by the last term of Eq. (27).

Nevertheless, none of these simple methods allow an accurate description of real systems. Pair interactions at

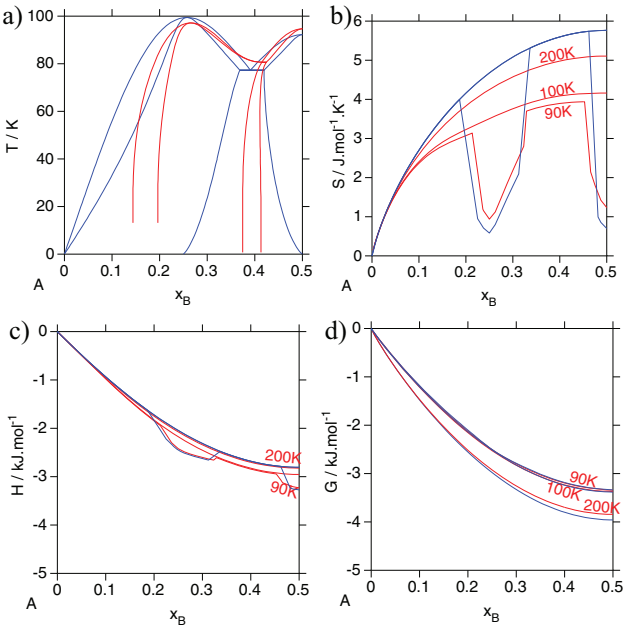

Figure 12 Comparison of the fcc prototype calculated by CVM in the tetrahedra approximation (red line) and with CEF using reciprocal interaction parameters Eq. (27) (blue line). In parts (a)–(d) the phase stability, entropy, enthalpy and Gibbs energy are shown versus concentration.

longer range and asymmetries have to be taken into account. This can properly be done with the CEF formalism as shown in the Au–Cu system, where all the ordered fcc structures appear as stable phases [148], or in the Al–Fe [149], where the $D0_3$ and B2 ordering were modelled together with the A2 disorder coupled with the magnetic ordering of these different phases.

5.4 Limitations Even if the introduction of reciprocal interaction parameters allows to get closer to the CVM approach, the SRO treatment of the CEF implementation has some limitations. Figure 12 compares, in addition to the phase diagram, the configurational entropy, ordering enthalpy and ordering Gibbs energy calculated by CVM and CEF using the same pair bond energy u. In Fig. 12b, the CVM and CEF configurational entropies are very close in the ordered state, even if the calculation has been made at 90 K, i.e. very close to the critical temperature. In the disordered state, while the CVM entropy, in red, progressively increases with temperature, the CEF value does not depend on the temperature.

Similar remarks hold for the ordering enthalpy in Fig. 12c: Independent of the temperature, the value for the disordered state is identical. At low temperatures the enthalpy of mixing is underestimated. The important differences observed at 100 K on the configurational entropy and on the enthalpy are somehow cancelling when it comes to the ordering Gibbs energy (Fig. 12d). In this figure, the calculations for 200 K – i.e. a temperature twice the critical temperature – show the largest difference, which is mostly due to the entropy difference at this temperature. These differences are closely related to the nature of the two approaches. They become significant when considering the derivatives of these functions, like the heat capacity. Therefore, in order to correctly describe the tail of the lambda transition, more complex terms must to be introduced in the CEF.

5.5 Experimental studies Figure 13 shows with the $Fe_{50}Co_{50}$ ferromagnetic alloy another example of a CALPHAD simulation using the CEF with reciprocal interaction parameters as well as a magnetic contribution according to the IHJ model [150, 151]. It contains in addition experimental data of the heat capacity. As already mentioned in Section 2.4, lambda transitions, as the present one, can in principle be measured by thermal analysis (see Fig. 5). However, the determination of order–disorder transition temperatures with this technique is difficult, if the slope of the transition boundary is steep. In such a situation, the diffusion couple technique is an effective alternative to determine the order–disorder transition composition at a certain temperature [152].

This shall be explained for the example of an Fe–Si system. Figure 14a shows an example of a back scattered electron image of a such a diffusion couple, which was heat-treated at 800 °C for 336 h. The chemical composition of Si across the diffusion layers were measured by a electron microprobe analyser (FE-EMPA). Figure 14b and c shows

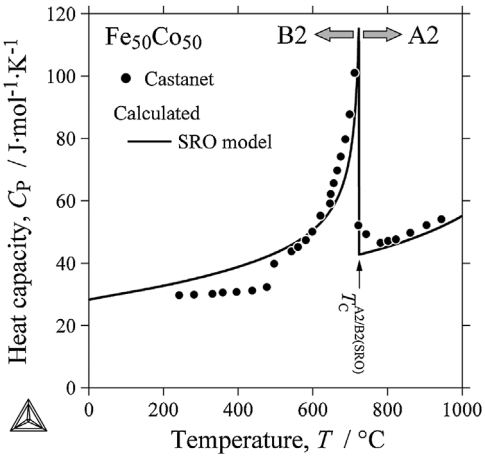

Figure 13 Experimental results for the molar heat capacity of the equiatomic Fe–Co alloy [150] in comparison with the results of a CEF calculation with reciprocal interaction parameters (solid line) [151].

the results of the measurement on two diffusion couples, Fe–8Si/Fe–23Si and Fe–13Si/Fe–23Si, which where heat-treated at 800 and at 1000 °C, respectively.

In the Si composition profile shown in Fig. 14b a composition gap and a kink were obtained, which correspond to the miscibility gap between the B2 (15.1 at% Si) and the $D0_3$ (15.8 at% Si) phases and to the A2/B2 second order transition boundary (12.5 at% Si), respectively. The kink of the Si composition profile is caused by the difference of the diffusivity of Si in the A2 disordered phase and the B2 ordered phase ($D_{Si}^{A2} > D_{Si}^{B2}$). In the Si composition profile shown in Fig. 14c, two kinks due to the A2/B2 (15.2 at% Si) and the B2/$D0_3$ (18.4 at% Si) boundaries were observed, which were also caused by $D_{Si}^{A2} > D_{Si}^{B2} > D_{Si}^{D03}$. The experimental results of these kind of experiments are summarized in Fig. 15 in comparison with the results of the CALPHAD assessment.

6 Coupling of degrees of freedom The previous sections of this paper are subdivided into a discussion of thermodynamic concepts for lambda transitions caused on the one hand by magnetic and on the other hand by chemical ordering. We have introduced the required simulation methods and have also pointed out similarities and differences between both degrees of freedom (DOF). Based on this information we can now extend the discussion to the interesting field of mutual interactions between these DOF.

One of the interesting aspects in this context is, for example, the effect of chemical order in an alloy on the magnetic critical temperature or the mean magnetic moment [153, 154]. This can in turn significantly influence the relative stability of different crystallographic phases in an alloy phase diagram. To account for these effects within the CALPHAD approach, one extend the IHJ model (Section 2) such that the parameters T_C and β depend on the degree of chemical order. Such an approach will be discussed below on the example of Fe–Al alloys.

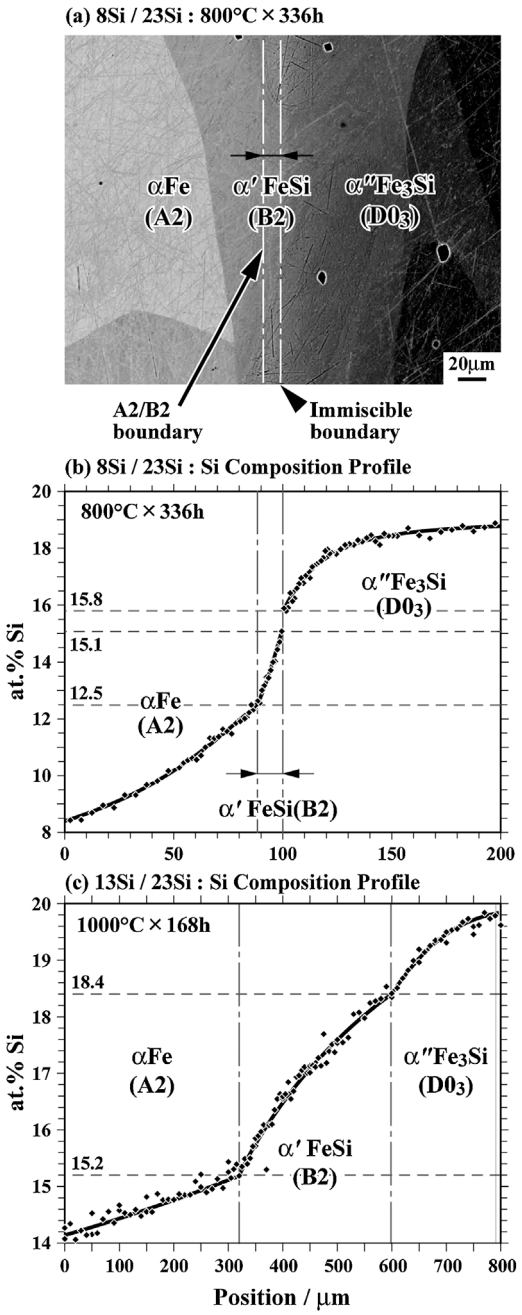

Figure 14 (a) BSE image and Si composition profiles of diffusion couples; (b) 8Si/23Si heat-treated at 800 °C and (c) 13Si/23Si at 1000 °C. Details can be found in Ref. [152].

A magnetic lambda transition can also affect structural properties directly. Based on the first-principles methodologies outlined in Section 3 we show how the delicate interplay between magnetic and atomic Gibbs energies together are responsible for the structural stability sequence in pure Fe. In addition several examples will be discussed, highlighting the effect of magnetic lambda transitions on various other materials properties. Eventually, the interplay between external pressure and magnetic DOF is discussed at the end of the section.

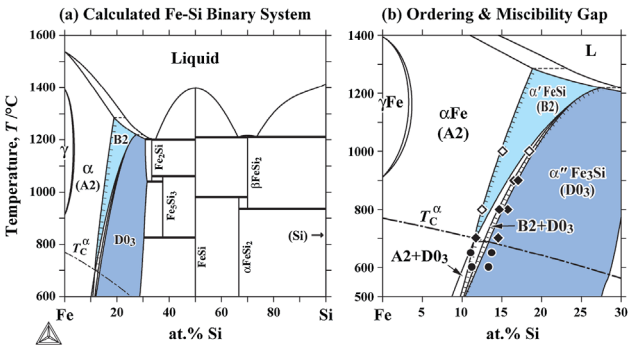

Figure 15 (a) Calculated phase diagrams of the Fe–Si binary system and (b) comparison with experimental data as obtained from diffusion couple experiments. Picture adapted from Ref. [152].

6.1 Coupling of chemical and magnetic DOF It has been realized already 25 years ago that the chemical interactions present in an alloy, sensitively depend on the global magnetic state [155]. One possibility to study chemical order–disorder transitions from first-principles directly is the investigation of the effective cluster interactions ECIs within the cluster expansion method (see also Section 5.2 and Ref. [96] for a recent review). In combination with the disordered local moment model (DLM) [156], which allows one to simulate the paramagnetic state, the ECIs provide an elegant way to study the impact of the magnetic state on the chemical order–disorder transitions. For $Co_{0.25}Pt_{0.75}$, where the chemical order–disorder transition takes place above the magnetic transition, i.e. in the paramagnetic regime, Ruban et al. showed that it is necessary to account for the presence of magnetic disorder in order to reproduce the experimental value [157]. In contrast, performing calculations in the ferromagnetic state yields values far off the experimental observation.

Even if the chemical order–disorder transition takes place below the magnetic transition, as for instance in FeCo and $FeNi_3$, it turns out to be mandatory to account for the partial loss of magnetic long-range order in the simulations [158, 159]. Based on the partial disordered local moment model (PDLM), Eckholm et al. [159] showed that the temperature induced deviation of the magnetic groundstate in $FeNi_3$ crucially influences the chemical transition temperature. A similar conclusion has been derived in Ref. [158], where the impact of the magnetic state on the ECIs has been studied in order to describe the ordering transition in Fe–Co alloys (see also Fig. 13).

If the coupling of the magnetic and chemical DOF is known (e.g. from first-principles investigations), one can also account for this effect within the CALPHAD approach. This requires to consider the chemical order dependence of the individual parameters entering the magnetic IHJ model, i.e. β and T_C. Before introducing two empirical deviation

parameters for these quantities, we illustrate the impact of chemical order on β and T_C on a few examples.

6.1.1 Effect on local magnetic moments β The delicate coupling of magnetic and chemical DOF is nicely exemplified by the Fe–V system. It is a well studied system, which has a B2 ordering tendency, can be prepared as a bcc solid solution in the whole composition range, and shows in addition magnetic phenomena. A phase diagram including the metastable A2 and B2 phases was calculated by Sanchez et al. [160] using the CVM (see also Section 5.2). Close to the equiatomic composition the chemical ordering vanishes at about 1150 K [161] and the magnetic Curie temperature is in the same temperature range [162], which makes an unambiguous determination of each temperature difficult. At low V concentrations, up to 20 at% V, the system is mostly chemically disordered. In this region, experimental [163, 164] and computational [165] studies show that the Fe magnetic moment stays the same as in pure Fe, or increases slightly. V atoms have a moment, that is antiferromagnetically aligned to the Fe atoms, and which decreases with increasing V content.

However, the magnitudes of the magnetic moments depend strongly on the degree of chemical ordering. For example, the measured magnetic moment per Fe atom β is about 1 μ_B for quenched (disordered) $Fe_{0.5}V_{0.5}$ [166], while heat-treated samples (ordered) were non-magnetic. Even at lower V concentrations the difference between quenched and heat-treated samples was substantial. *Ab initio* calculations confirm that the magnetic moment is larger in the chemical disordered phase [167], while finite β values are still reported for the ordered (B2) structure [168–170] . An available CALPHAD assessment for the Fe–V system from 1983 [171] accurately predicts the occurrence of a sigma phase as well as T_C for Fe-rich compositions and also shows that magnetism stabilizes the bcc phase with respect to the sigma phase. However, at that time the model was not able to account for ordering and its magnetic implications.

6.1.2 Effect on Curie temperature T_C It is well known that T_C of ordered compounds has different values than those of disordered solutions. For instance, T_C of the α''-Fe_3Al ($D0_3$) ordered phase in the Fe–Al system is suppressed compared to that of the α-Fe (A2) disordered phase at the same composition. A similar *atomic-order suppressed magnetism* is observed for the B2 ordering of bcc alloys in the Fe–V (discussed above) and Fe–Mn systems, and the $L1_0$ and $L1_2$ ordering of fcc alloys in the Ni–Pt and the Co–Pt systems [153]. On the other hand, the phase diagram of the Fe–Ni system indicates that T_C in a (metastable) γ'-$FeNi_3$ ($L1_2$) ordered compound has a higher value than that of the γ (A1) disordered solution [172] (see upward arrow). Similarly, the α'-FeCo (B2) and γ'-Ni_3Mn ($L1_2$) ordered compounds [153] fall into the category of *atomic-order enhanced magnetism*.

In consequence, the stability of the ordered phase is also suppressed (enhanced) due to the interaction between the chemical and magnetic DOF. Cadeville and Moran-Lopez [153] carried out in-depth investigations of these interaction of magnetism and spatial order in transition metal alloys. Their thermodynamic models and theoretical calculations show qualitative agreement with the experimental observations. In the present paper, we can therefore focus on some selected topics and on novel developments that allow one to obtain a better quantitative agreement.

6.1.3 Deviation parameters One important development for a better description of magnetic properties and evaluation of existing phase diagrams was the introduction of deviation parameters

$$\Delta T_{Co/d} = T_{Co} - T_{Cd} \quad \text{and} \quad \Delta\beta_{Co/d} = \beta_{Co} - \beta_{Cd} \tag{28}$$

into the ordinary CALPHAD method [151, 173]. Here, subscripts 'o' and 'd', correspond to chemically ordered and disordered states, respectively. The method has been in particular used for the investigation of the interaction effect between the chemical and magnetic ordering on the phase equilibria in the Fe–X (X = Al, Co, Ni) binary systems. These investigations have been performed, using the two- or four-sublattice split compound energy formalism (s-CEF) in the same way as for the ordering contribution to the Gibbs energy (see Section 5). The four sublattices are necessary for bcc alloys to distinguish the B2 and $D0_3$ structures, when considering first and second nearest-neighbour interactions. Similarly, the fcc structures A1, $L1_0$ and $L1_2$ also require four sublattices taking into account first nearest-neighbour interactions. The corresponding parameters in the Gibbs energy expressions are provided in Ref. [173]. The magnetic properties of disordered phases are described neglecting the chemical interaction terms.

We first discuss how the magnetic contribution to the Gibbs energy in a hypothetical A–B binary bcc alloy is analysed using the s-CEF approach. We assume constituent atom A to be ferromagnetic with $T_{CA} = 1000$ K and $\beta_A = 2\ \mu_B$, while the constituent atom B is assumed to be non-magnetic, i.e. $T_{CB} = 0$ K and $\beta_B = 0\ \mu_B$.

More specifically, $\Delta T_C^{B2/A2}$ represents in the spirit of Eq. (28) the maximum deviation of T_C between the disordered A2 and the fully ordered B2 phase at the composition of $x_A = x_B = 0.5$ as shown in Fig. 16a. Here the deviation of T_C is shown as a function of the degree of chemical LRO for values of $\Delta T_C^{B2/A2}$ = 0, −250 and +250 K. The magnetic contribution to the Gibbs energy changes is illustrated in Fig. 16b. Furthermore, the total Gibbs energies including the interaction (solid lines) deviate from the ones without the interaction (thick dashed line) as shown in Fig. 16c. As a result, the most stable ordering state (indicated by solid circles in Fig. 16d) changes depending on the interaction, which will have an impact on the phase diagram.

In the absence of any magnetic interaction with the chemical ordering, the calculated diagram, corresponding to the hypothetical A–B binary system exhibits the simple

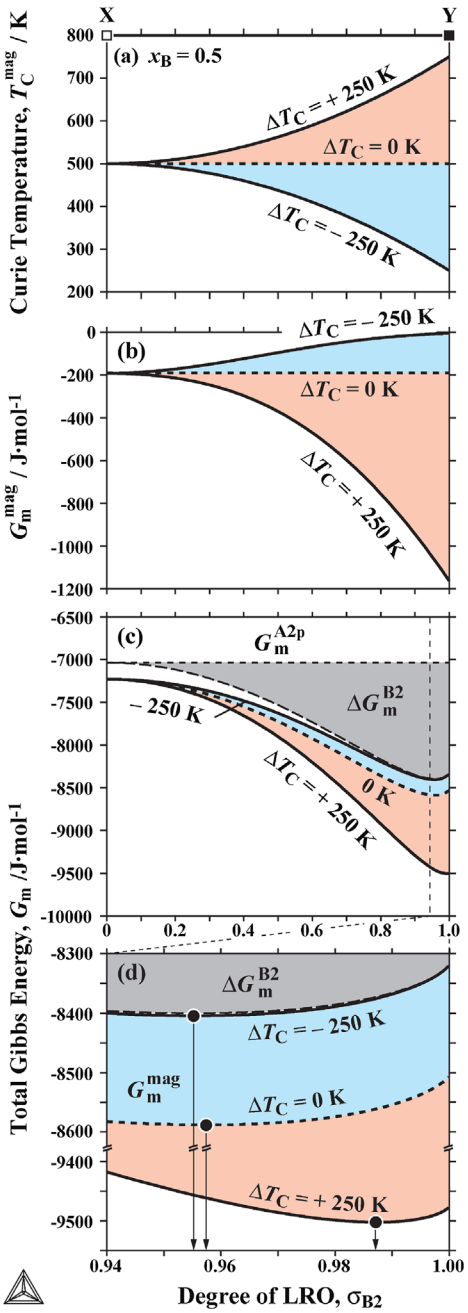

Figure 16 Deviations of (a) Curie temperature, (b) magnetic contributions to the Gibbs energy, (c) and (d) total Gibbs energies for different values of ΔT_C. The most stable degree of LRO changes as a result of the interaction.

configuration diagram shown in Fig. 17(a2). In addition the Gibbs energy curves at 500 K are shown in Fig. 17(a1).

After introducing the magnetic interaction parameter $\Delta T_C^{B2/A2} = -250$ K, we show the subsequently calculated Gibbs energies at 500 K and the phase diagram in Fig. 17b. The thick curve in Fig. 17(b1) represents the total calculated Gibbs energy including the magnetic–chemical interaction, which loses both, the chemical and the magnetic, ordering contributions. This renders the B2 ordered structure less stable after introducing the magnetic interaction, which is reflected by a lower degree of distortion of the A2/B2 boundary shown in Fig. 17(b2). The interaction between magnetic and chemical ordering components, therefore, leads to a depression of the ordering reaction and manifests itself as a decrease in the area of overlap between chemical and magnetic ordering contributions to the Gibbs energy shown in Fig. 17(b1). The resulting total Gibbs energy curve exhibits an upward convex shape across the compositions in the vicinity of the intersection point, and a two-phase equilibrium between the $A2_p$ and the $B2_p$ phases opens along the A2/B2 boundary consisting of a tri-critical point. The constituent phases of this two-phase equilibrium change in the following order as the temperature is lowered: to the $A2_f$ and the $B2_p$ and, finally to the $B2_f$ and the $B2_p$ phases as the boundary closes along the T_C curve of the ordered B2 structure.

On the other hand, when T_C is pushed up to a higher value by 250 K in the fully ordered state, i.e. $\Delta T_C^{B2/A2} = +250$ K, the ordering reaction is seen to raise T_C as shown in Fig. 17(c2), which in turn causes an enhanced gain in the magnetic contribution to the Gibbs energy as shown in Fig. 17(c1). As a consequence, the chemical ordering is enhanced even though the transition causes loss of the Gibbs energy and the region associated with the B2 ordered structure expands in the vicinity of the intersection point between the A2/B2 boundary and the T_C curve. The stabilization of the B2 ordered structure is also reflected in the appearance of a convex surface in the Gibbs energy curve at the B-rich side, which gives rise to two phase equilibria, one between the $B2_f$ and the $B2_p$ phases along T_C, which turns into a second equilibrium between the $B2_f$ and the $A2_p$ phases at a lower temperature.

6.1.4 Application Having discussed different hypothetical scenarios of how chemical and magnetic DOF can influence the phase stabilities, we now turn to the application to an Fe-alloy, namely the Fe–Al binary system. As mentioned above, the interaction between magnetic and chemical ordering is experimentally observed in several Fe–X (X = Co, Al, Ni etc.) binary systems. In the Fe–Al system the nature of the A2/B2/$D0_3$ phase equilibria is categorized as double interactive interchange energies, i.e. $W_{AB}^{(1)} > 0$ and $W_{AB}^{(2)} > 0$, in the BWG theory (see Section 5). In the vicinity of the intersection point between the A2/B2 boundary and T_C, however, a A2 + B2 phase separation coexists, which is manifestly inconsistent with the underlying theory. Therefore, special attention should be paid to the incorporation of the deviation of magnetic properties due to chemical ordering, in particular in view of the experimental results indicating a magnetic depression as shown in Fig. 17b. Figure 18 shows the results (a) without and (b) with inclusion of the interaction effect on the bcc phase equilibria in the Fe–Al system [175]. The interaction of chemical and magnetic DOF is responsible for the decrease of the magnetic properties ($\Delta T_{Co/d} = -350$ K and $\Delta\beta_{o/d} = -1.2\mu_B$). Consequently, the depressed interaction causes the loss of both, the magnetic and chemical, ordering contributions. This results

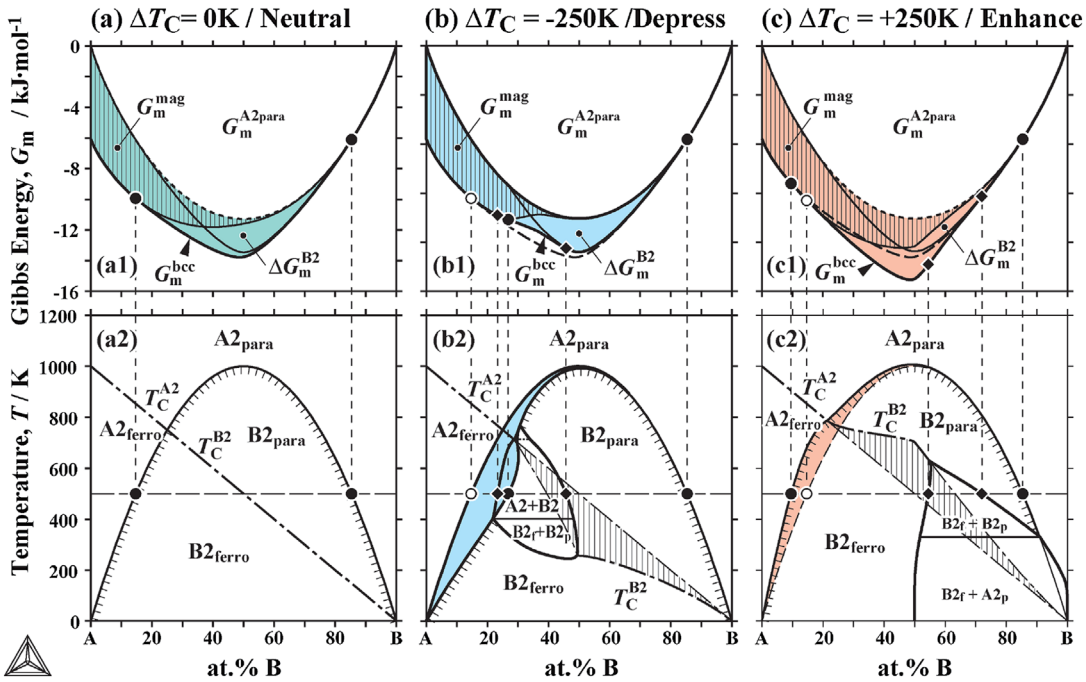

Figure 17 Gibbs energy at 500 K and phase diagrams for A2/B2 transition and phase separations showing the effect of the Curie temperature deviation [151]. The interaction between magnetic and chemical DOF are taken into account for (a) vanishing magnetic interaction, (b) enhancing magnetic interaction, (c) suppressing magnetic interaction.

in a convex on the total Gibbs energy curve similar to that in Fig. 17(b1). As a consequence, an A2 + B2 phase separation opens in the vicinity of the intersection point and turns into an A2 + $D0_3$ separation at low temperatures as shown in Fig. 18b. It has been reported that this A2 + $D0_3$ separation extends with decreasing temperature [176].

6.2 Relevance of lambda transitions for other Gibbs energy contributions As discussed above, the coupled magnetic and chemical DOF can substantially influence alloy phase stabilities. We should also point out that already the magnetic transitions alone can have a dramatic effect on phase stability. This (relative) stability is determined by the difference between the *total* (i.e. containing the magnetic plus all the other terms) Gibbs energies. One of the striking plays a pivotal part is the structural stability and phase transitions in pure iron (Fe).

Iron exhibits two structural phase transitions, one from bcc to fcc phase at 1184 K, and one back into bcc phase at 1678 K, before it melts at about 1811 K. It is well known

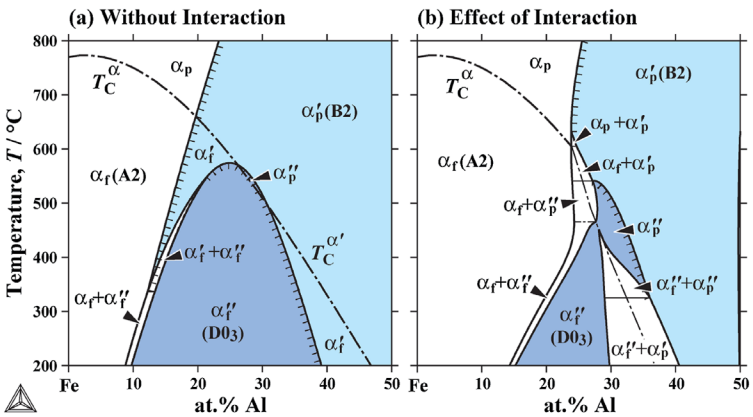

Figure 18 Partial phase diagrams of the Fe–Al binary system (a) without and (b) with considering the effect of the interaction. The interaction causes the α (A2) + α' (B2) two-phase separation. Picture adapted from Ref. [174]: I. Ohnuma, R. Kainuma, and K. Ishida, "Effect of the Interaction between the Chemical and the Magnetic Ordering on the Phase Equilibria of Iron-base Alloys," in CALPHAD and Alloy Thermodynamics (2002), P.E.A. Turchi, A. Gonis, and R.D. Shull, eds., p. 75, Figure 14. Copyright © 2002 by The Minerals, Metals & Materials Society. Reprinted with permission.

that magnetism is of utmost importance for these structural changes [5]. Extensive theoretical effort spanning several decades has been dedicated to explaining and interpreting phase transitions in iron. Theoretical work included applications of a semi-empirical two-states model (see, e.g. in Ref. [177]), microscopic band theories [178], and dynamical mean field calculations [179]. Despite the considerable theoretical and computational effort, the question about the balance between various entropic contributions (vibrational and electronic/magnetic) to the phase transition has not been resolved. Whereas the treatment of electronic/magnetic contributions always received attention, vibrational contributions were usually neglected [178, 179]. One of the rare high temperature experiments on fcc Fe showed that the Debye temperature of fcc Fe of ≈324 K is lower than the corresponding temperature of bcc Fe (≈420 K) [180], indicating that the vibrational Gibbs energy contribution helps to stabilize fcc Fe at high temperature. [6]

In order to elucidate the impact of the Curie magnetic lambda transition in Fe on its structural stability we present in Fig. 19 two independent theoretical models for the bcc–fcc internal energy and free energy differences. Details of the calculations are given elsewhere [76, 182]. Both theoretical approaches clearly emphasize the pivotal significance of electronic/magnetic effects for the phase stability. Similarly, both models also consistently predict vibrational contributions to be of crucial importance for the stabilization of fcc Fe, in agreement with the experimental Debye temperature measurements. Noting a broad range of methodological challenges described in Section 3, we point out that including all the Gibbs energy contributions in a consistent theoretical framework is a highly non-trivial task, making quantitative prediction of structural stability a genuine challenge. Nevertheless, both models, illustrated in Fig. 19, are able to capture the occurrence of *two* structural transitions in iron, and agree on the detailed balance between the free energy contributions resulting from electronic/magnetic and atomic/vibrational degrees of freedom.

In Fe, structural transitions are closely linked to the magnetic lambda transition. A magnetic order–disorder transition affects the motion of atoms, and hence the vibrational contribution to the Gibbs energy. A fundamental reason for that is the fact that interatomic forces depend on the magnetic state and this in turn results in a significant variation of the vibrational Gibbs energy. A prominent example is bcc Fe [183–186]. It has been recognized a long time ago that the tetragonal shear modulus C' softens as iron approaches the Curie temperature (see, e.g. [187]). This is a precursor for the bcc to fcc transition, which occurs at 1184 K.

[6] Following pure geometric arguments one might assume bcc Fe to have a lower Debye temperature than its corresponding fcc crystal phase. In combination with magnetic effects, however, such an assertion is no longer valid. One reason for this is that interatomic forces strongly depend on the magnetic state (see Fig. 20) and on the magnitude of local atomic magnetic moments, as exemplified in Ref. [181] by a computation of the phonon spectra within a fixed spin moment approach.

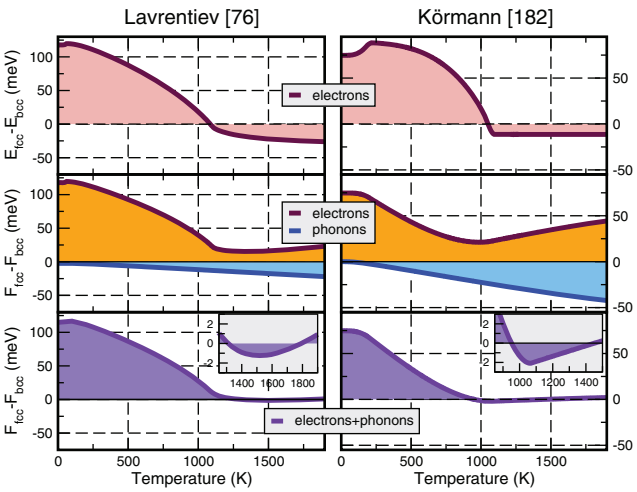

Figure 19 Results of calculations illustrating applications of two independently developed theoretical models for structural stability and bcc–fcc–bcc sequence of phase transitions in Fe [76, 182]. The first row shows the difference between the internal energies of the two phases, the second row shows the free energy differences, and the last row the total (electronic/magnetic plus vibrational) free energy differences between fcc and bcc phases of Fe.

Consequently one observes a pronounced softening of the phonon modes associated with such transition. The fact that this is a direct consequence of the magnetic lambda transition is illustrated in Fig. 20. In this figure, recent DFT data are compared with the high temperature experimental data. Theoretical calculations were performed for the ferromagnetic (i.e. magnetically ordered) and paramagnetic (magnetically disordered) cases. Apart from the good agreement with experiment, the paramagnetic calculations clearly show the strong effect of the magnetic lambda transition on atomic motion. From such phonon calculations the harmonic vibrational free energy can be computed in a straightforward manner [11], resulting in approximately 10% reduction of the vibrational free energy caused by the loss of magnetic order. This reveals a clear link between magnetic lambda transitions

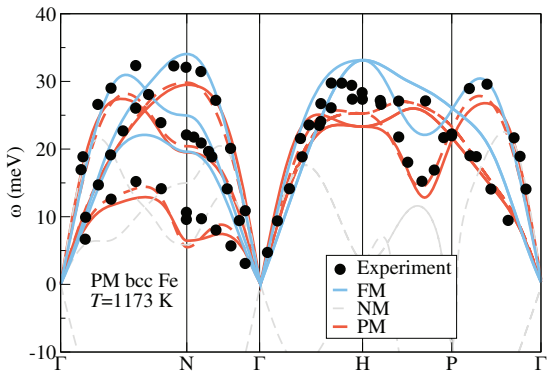

Figure 20 Theoretical and experimental phonon spectra of bcc Fe at 1173 K. The magnetic lambda transition is responsible for the strong softening of C' observed in experiment. Picture adapted from Ref. [186].

and the vibrational Gibbs energy, and consequently between magnetic lambda transitions and structural transitions, on a quantitative level.

The softening of C' also has a strong effect on the temperature dependence of anisotropic elastic self-energies of dislocations in iron [188]. For example, the difference between anisotropic elastic free energies of the $a\langle 100\rangle$ and $a/2\langle 111\rangle$ prismatic edge dislocation loops explains the observed dominant occurrence of the $a\langle 100\rangle$, as opposed to the $a/2\langle 111\rangle$, Burgers vector configurations of prismatic loops in iron at high temperature [188]. These theoretical predictions have now been confirmed experimentally [189].

The magnetic lambda transition also has a dramatic effect on the vacancy formation and migration energies and (self)-diffusion in Fe and Fe–Cr alloys [185, 190]. In Ref. [185] the vacancy formation energies in bcc Fe were computed employing various theoretical approaches. In all the cases investigated in Ref. [185] a dramatic reduction of the vacancy formation energy was observed for the paramagnetic as opposed to the ferromagnetic (ground state) calculations. In Ref. [190] the rate of diffusion of Cr and self-diffusion of Fe in bcc Fe was investigated by means of kinetic Monte Carlo simulations. Analysis shows that the experimentally observed dramatic (nearly two orders of magnitude) increase of the self-diffusion coefficients around the magnetic transition temperature cannot be explained if one neglects the magnetic entropy effects. Further details on current modelling of (point) defects can be found elsewhere [83].

As discussed in Section 6.1, in iron-based magnetic alloys both the lambda transitions and structural transitions are sensitive to the chemical composition of the alloys. For example, in binary Fe–Cr alloys the Curie temperature, treated as a function of Cr concentration, first rises, reaching a maximum at approximately 6% Cr [191], and then rapidly decreases. As Cr concentration increases, the temperatures of the bcc–fcc and fcc–bcc structural transitions converge, and in alloys containing in excess of 11.9% Cr the high-temperature fcc phase is unstable at all temperatures [76]. Phase decomposition and formation of Cr precipitates in high-Cr alloys results in a large variation of the magnetic lambda transition temperature, which appears highly sensitive to alloy microstructure [192].

7 Conclusions Recent advances and state-of-the-art methods in computational guided materials design, addressing chemical and magnetic order–disorder (often called lambda) transitions, are discussed. A comprehensive overview is given of the related CALPHAD and first-principles methods to describe the relevant Gibbs energy contributions. Critical questions are addressed, for example how CALPHAD and first-principles methods can be interlinked and what are the potential issues and limitations. Since the ultimate goal of the thermodynamic simulations is the prediction of measurable quantities, a substantial part of the paper is devoted to currently available experimental data and techniques.

The CALPHAD approach requires evaluating the Gibbs energy of phases including the effect of an internal (or spontaneous) magnetization and of chemical ordering of atoms. Since the seminal work of Inden–Hillert–Jarl (IHJ) [6], no major attempt has been made to replace the magnetic model by a more physically justified one. Therefore, the performance of the IHJ-based approaches is discussed in detail including its validity range, physical limiting cases, and the interpretation of the parameters. One of the outcomes is that the parameters entering the IHJ model, such as, e.g. the mean magnetic moment β, can imply under certain circumstances a rather different meaning as opposed to values obtained from first-principles methods directly. In particular when applied to alloy systems showing multi-magnetic phases, the analytic description of the IHJ model parameters needs to be adapted as exemplified for an alloy exhibiting a FM to AFM composition dependent magnetic transition.

We have also documented in this article, that complementary to the CALPHAD description, substantial progress has been recently made to achieve an *ab initio* description of magnetism at finite temperatures. The treatment of magnetic contributions is introduced using microscopic model Hamiltonians (Hubbard model, Heisenberg model and beyond). A fundamental difference between the empirical analytic IHJ model and the physically motivated model Hamiltonians is that in most cases the latter cannot be solved within a mathematically closed analytic expression and require rather sophisticated solution techniques (e.g. Quantum Monte Carlo methods). This makes the direct implementation of the model Hamiltonians within CALPHAD often impossible. Instead, we suggest as a possible exploitation of the described methods and results to supplement experimental data as *virtual experiments*.

Based on the insights obtained from the CALPHAD and the *ab inito* approaches, we were able to derive several guidelines for the derivation of physically, yet in CALPHAD practically implementable methods to thermodynamically model magnetism. This includes physical foundations, such as the knowledge of the behaviour in limit cases, such as critical exponents and low temperature limits. We point out possible conceptional difficulties related to a separation of magnetism and advert alternative magnetic models, such as approaches based on Landau-type parameterizations.

In parallel to the magnetic discussion, computational schemes capturing atomic order–disorder effects such as the Bragg–Williams based approaches and the cluster variation method are discussed. Limitations and recent advances are illustrated with selected examples. The discussion revealed several interlinks between both physical phenomena, which could be used in future to mutually benefit from developments in both fields. The applicability of the CVM to describe chemical *and* magnetic order–disorder processes could be one example.

An important consequence of the knowledge of the treatment for both, magnetic and chemical degrees of freedom within the CALPHAD formalism, is the handling of coupling effects. It is shown how this coupling can be incorporated into the current CALPHAD approach by introducing chemical order-dependent correction factors for the IHJ parameters β

and T_C. The application is illustrated using the Fe–Al alloy as test case. In addition, first-principles techniques and results are presented in order to resolve the interplay between magnetic and atomic degrees of freedom. Finally, the balance of atomic and magnetic Gibbs energy contributions to phase stabilities is discussed for pure Fe as an example.

Acknowledgements One of us (GG) acknowledges support from the US Department of Energy (DOE), Office of Fossil Energy, under Grant No. DE-FG00568, with Richard Dunst as the program manager. Work at CCFE was funded by the RCUK Energy Programme under grant EP/I501045 and the European Communities under the Contract of Association between EURATOM and CCFE. The views and opinions expressed herein do not necessarily reflect those of the European Commission. Funding by the collaborative research center SFB 761 'Stahl – *ab initio*' of the Deutsche Forschungsgemeinschaft and the Interdisciplinary Centre for Advanced Materials Simulation (ICAMS), which is supported by ThyssenKrupp AG, Bayer MaterialScience AG, Salzgitter Mannesmann Forschung GmbH, Robert Bosch GmbH, Benteler Stahl/Rohr GmbH, Bayer Technology Services GmbH and the state of North-Rhine Westphalia as well as the European Commission in the framework of the European Regional Development Fund (ERDF), is gratefully acknowledged. Discussions with Igor A. Abrikosov, Gerhard Inden, Marcel H.F. Sluiter and Wei Xiong are gratefully acknowledged.

References

[1] W. H. Keesom and A. P. Keesom, Verh. K. Akad. Wet. (Amsterdam) **35**, 736 (1932).
[2] Q. Chen and B. Sundman, J. Phase Equilib. **22**(6), 631–644 (2001).
[3] D. de Fontaine, S. G. Fries, G. Inden, P. Miodownik, R. SchmidFetzer, and S. Chen, Calphad **19**(4), 499–536 (1995).
[4] G. Inden, Proc. Calphad V, 1–13 (1976).
[5] R. J. Weiss and K. J. Tauer, Phys. Rev. **102**, 1490–1495 (1956).
[6] M. Hillert and M. Jarl, Calphad **2**(3), 227–238 (1978).
[7] G. Inden, Physica **103B**, 82 (1981).
[8] S. Hertzman and B. Sundman, Calphad **6**, 67 (1982).
[9] W. Xiong, Q. Chen, P. A. Korzhavyi, and M. Selleby, Calphad **39**, 11 (2012).
[10] M. van Schilfgaarde, I. A. Abrikosov, and B. Johansson, Nature **400**, 46 (1999).
[11] M. Palumbo, B. Burton, A. C. de Silva, B. Fultz, B. Grabowski, G. Grimvall, B. Hallstedt, O. Hellmann, B. Lindahl, A. Schneider, P. E. A. Turchi, and W. Xiong, Phys. Status Solidi B **251**, 14–32 (2014), this issue.
[12] Y. Tsunoda, J. Phys.: Condens. Matter **3**, 7231 (1991).
[13] Y. Tsunoda, J. Phys.: Condens. Matter **1**(51), 10427 (1989).
[14] M. Straub, R. Vollmer, and J. Kirschner, Phys. Rev. Lett. **77**, 743 (1996).
[15] A. Knappwost and G. Bockstiegel, Z. Elektrochem. **57**, 700 (1953).
[16] S. C. Abrahams, L. Guttman, and J. S. Kasper, Phys. Rev. **127**, 2052–2055 (1962).
[17] M. Marsman and J. Hafner, Phys. Rev. B **66**(22), 224409 (2002).
[18] V. Sedov, Sov. Phys. – JETP **15**, 88 (1962).
[19] H. Umebayashi and Y. Ishikawa, J. Phys. Soc. Jpn. **21**, 1281 (1966).
[20] Y. Ishikawa and Y. Endoh, J. Phys. Soc. Jpn. **23**, 205 (1967).
[21] T. Hashimoto and Y. Ishikawa, J. Phys. Soc. Jpn. **23**, 213 (1967).
[22] Y. Ishikawa and Y. Endoh, J. Appl. Phys. **39**(2), 1318–1319 (1968).
[23] Y. Endoh and Y. Ishikawa, J. Phys. Soc. Jpn. **30**, 205 (1971).
[24] R. J. Weiss and K. J. Tauer, Phys. Rev. **102**, 1490–1495 (1956).
[25] A. Miodownik, Scr. Metall. **3**, 931 (1969).
[26] Y. Nakamura, M. Shiga, and N. Shikazono, J. Phys. Soc. Jpn. **19**, 1177 (1964).
[27] Y. Nakamura, Y. Takeda, and M. Shiga, J. Phys. Soc. Jpn. **25**, 287 (1968).
[28] N. Kamiya, I. Ohnuma, R. Kainuma, and K. Ishida, unpublished.
[29] R. Wayne and L. Bartel, Phys. Lett. **28A**, 196 (1968).
[30] Y. Nakamura, M. Hayase, M. Shiga, Y. Yamamoto, and N. Kawai, J. Phys. Soc. Jpn. **30**, 720 (1971).
[31] J. Noakes, H. Sato, and A. Arrort, J. Appl. Phys. **42**, 1608 (1971).
[32] T. Hammerschmidt, I. A. Abrikosov, D. Alfé, S. G. Fries, L. Höglund, M. H. G. Jacobs, J. Koßmann, X.-G. Lu, and G. Paul, Phys. Status Solidi B **251**, 81–96 (2014), this issue.
[33] P. W. Anderson, Phys. Rev. **124**, 41–53 (1961).
[34] J. Hubbard, Proc. R. Soc. Lond. A, Math. Phys. Sci. **276**(1365), 238–257 (1963).
[35] G. Kotliar, S. Y. Savrasov, K. Haule, V. S. Oudovenko, O. Parcollet, and C. A. Marianetti, Rev. Mod. Phys. **78**, 865–951 (2006).
[36] J. Griffith, The Theory of Transition Metal Ions, first ed. (Cambridge University Press, Cambridge, UK, 1961).
[37] Z. Rudzikas, Theoretical Atomic Spectroscopy (Cambridge University Press, Cambridge, UK, 1997).
[38] P. Fazekas, Electron Correlations and Magnetism (World Scientific, Singapore, 1999).
[39] A. I. Liechtenstein, V. I. Anisimov, and J. Zaanen, Phys. Rev. B **52**, R5467–R5470 (1995).
[40] A. Kotani and T. Yamazaki, Prog. Theor. Phys., Suppl. **108**, 117 (1992).
[41] S. L. Dudarev, G. A. Botton, S. Y. Savrasov, C. J. Humphreys, and A. P. Sutton, Phys. Rev. B **57**, 1505–1509 (1998).
[42] S. L. Dudarev, G. A. Botton, S. Y. Savrasov, Z. Szotek, W. M. Temmerman, and A. P. Sutton Phys. Status Solidi A **166**(1), 429–443 (1998).
[43] D. Nguyen-Manh and S. L. Dudarev, Phys. Rev. B **80**, 104440 (2009).
[44] D. J. Kim, New Perspectives in Magnetism of Metals (Springer, New York, 1999).
[45] M. Coury, S. Dudarev, W. Foulkes, A. Horsfield, and P. W. Ma, unpublished (2013).
[46] P. Fulde, Electron Correlations in Molecules and Solids, third ed., Springer Series in Solid-State Sciences, Vol. 100 (Springer, Berlin, 1995).
[47] A. Liechtenstein, M. Katsnelson, V. Antropov, and V. Gubanov, J. Magn. Magn. Mater. **67**(1), 65–74 (1987).
[48] L. M. Sandratskii, Phys. Status Solidi B **136**(1), 167–180 (1986).
[49] M. Pajda, J. Kudrnovsky, I. Turek, V. Drchal, and P. Bruno, Phys. Rev. B **64**, 174402 (2001).

[50] N. M. Rosengaard and B. Johansson, Phys. Rev. B **55**, 14975 (1997).
[51] M. Ležaić, P. Mavropoulos, and S. Blügel, Appl. Phys. Lett. **90**, 082504 (2007).
[52] A. V. Ruban, S. Khmelevskyi, P. Mohn, and B. Johansson, Phys. Rev. B **75**, 054402 (2007).
[53] J. Rusz, L. Bergqvist, J. Kudrnovský, and I. Turek, Phys. Rev. B **73**, 214412 (2006).
[54] G. Y. Gao, K. L. Yao, E. Şaşioğlu, L. M. Sandratskii, Z. L. Liu, and J. L. Jiang, Phys. Rev. B **75**, 174442 (2007).
[55] F. Körmann, A. Dick, T. Hickel, and J. Neugebauer, Phys. Rev. B **79**, 184406 (2009).
[56] F. Körmann, A. Dick, T. Hickel, and J. Neugebauer, Phys. Rev. B **81**(13), 134425 (2010).
[57] W. Heisenberg, Z. Phys. **49**(9–10), 619–636 (1928).
[58] P. A. M. Dirac, Proc. R. Soc. Lond. A **118**(779), 351–361 (1928).
[59] M. Exler, On Classical and Quantum Mechanical Energy Spectra of Finite Heisenberg Spin Systems, Ph.D. thesis, University Osnabrück (2006).
[60] P. W. Ma and S. L. Dudarev, Phys. Rev. B **86**, 054416 (2012).
[61] J. Oitmaa and W. Zheng, J. Phys.: Condens. Matter **16**(47), 8653 (2004).
[62] W. Nolting and A. Ramakanth, Quantum Theory of Magnetism (Springer, Berlin, 2008).
[63] A. W. Sandvik and J. Kurkijärvi, Phys. Rev. B **43**(7), 5950–5961 (1991).
[64] H. G. Evertz, Adv. Phys. **1**, 1 (2003).
[65] P. Henelius and A. W. Sandvik, Phys. Rev. B **62**(2), 1102–1113 (2000).
[66] E. Y. Loh, J. E. Gubernatis, R. T. Scalettar, S. R. White, D. J. Scalapino, and R. L. Sugar, Phys. Rev. B **41**(13), 9301–9307 (1990).
[67] L. Bergqvist, B. Belhadji, S. Picozzi, and P. H. Dederichs, Phys. Rev. B **77**(1), 014418 (2008).
[68] F. Körmann, A. Dick, B. Grabowski, B. Hallstedt, T. Hickel, and J. Neugebauer, Phys. Rev. B **78**, 033102 (2008).
[69] F. Körmann, A. Dick, T. Hickel, and J. Neugebauer, Phys. Rev. B **83**(16), 165114 (2011).
[70] T. Hickel, B. Grabowski, F. Körmann, and J. Neugebauer, J. Phys.: Condens. Matter **24**(5), 053202 (2012).
[71] A. Dick, F. Körmann, T. Hickel, and J. Neugebauer, Phys. Rev. B **84**, 125101 (2011).
[72] R. Drautz and M. Fähnle, Phys. Rev. B **72**, 212405 (2005).
[73] R. Singer, F. Dietermann, and M. Fähnle, Phys. Rev. Lett. **107**, 017204 (2011).
[74] H. Capellmann, J. Magn. Magn. Mater. **28**(3), 250–260 (1982).
[75] M. Lavrentiev, S. Dudarev, and D. Nguyen-Manh, J. Nucl. Mater. **386–388**, 22–25 (2009).
[76] M. Y. Lavrentiev, D. Nguyen-Manh, and S. L. Dudarev, Phys. Rev. B **81**, 184202 (2010).
[77] P. M. Derlet, Phys. Rev. B **85**, 174431 (2012).
[78] P. W. Ma, C. H. Woo, and S. L. Dudarev, Phys. Rev. B **78**(Jul), 024434 (2008).
[79] P. W. Ma and C. H. Woo, Phys. Rev. E **79**, 046703 (2009).
[80] P. W. Ma, S. L. Dudarev, A. A. Semenov, and C. H. Woo, Phys. Rev. E **82**, 031111 (2010).
[81] P. W. Ma and S. L. Dudarev, Phys. Rev. B **83**(Apr), 134418 (2011).
[82] M. Y. Lavrentiev, R. Soulairol, C. C. Fu, D. Nguyen-Manh, and S. L. Dudarev, Phys. Rev. B **84**, 144203 (2011).
[83] J. Rogal, S. Divinski, M. W. Finnis, A. Glensk, J. Neugebauer, J. H. Perepezko, S. Schuwalow, M. H. F. Sluiter, and B. Sundman, Phys. Status Solidi B **251**, 97–129 (2014), this issue.
[84] M. J. Gillan, Contemp. Phys. **38**(2), 115–130 (1997).
[85] G. Ghosh, unpublished research, Northwestern University (2013).
[86] M. Fallot, Ann. Phys. (France) **11e**, 305 (1936).
[87] C. Shull and M. K. Wilkinson, Phys. Rev. **97**, 304 (1955).
[88] M. Nevitt and A. Aldred, J. Appl. Phys. **34**, 463 (1963).
[89] A. Aldred, Phys. Rev. B **14**, 219 (1976).
[90] Y. Dorofeyev, A. Z. Menshikov, and G. Takzey, Phys. Met. Metallogr. **55**, 102 (1983).
[91] J. Blacktop, J. Crangle, and B. Argent, Mater. Sci. Technol. **1**, 448 (1985).
[92] P. Weiss and R. Ferrer, Ann. Phys. (France) **12**, 279 (1929).
[93] M. Collins and J. Forsyth, Philos. Mag. **8**, 401 (1963).
[94] D. Bardos, J. Appl. Phys. **40**, 1371 (1969).
[95] A. van de Walle and G. Ceder, J. Phase Equilib. **23**(4), 348–359 (2002).
[96] A. V. Ruban and I. Abrikosov, Rep. Prog. Phys. **71**(4), 046501 (2008).
[97] P. Olsson, I. Abrikosov, and J. Wallenius, Phys. Rev. B **73**, 104416 (2006).
[98] P. James, O. Eriksson, B. Johansson, and I. A. Abrikosov, Phys. Rev. B **59**, 419–430 (1999).
[99] G. Ghosh, A. van de Walle, and M. Asta, Acta Mater. **56**, 3202 (2008).
[100] G. Kresse and J. Furthmüller, Phys. Rev. B **54**, 11169–11186 (1996).
[101] P. E. Blöchl, Phys. Rev. B **50**(24), 17953 (1994).
[102] J. P. Perdew, J. Chevary, S. Vosko, K. A. Jackson, M. R. Pederson, D. Singh, and C. Fiolhais, Phys. Rev. B **46**(11), 6671 (1992).
[103] R. Richter and H. Eschrug, J. Phys. F, Met. Phys. **18**, 1813 (1988).
[104] M. van Schilfgaarde, I. Abrikosov, and B. Johansson, Nature **400**(6739), 46–49 (1999).
[105] E. Şaşıoğlu, L. M. Sandratskii, P. Bruno, and I. Galanakis, Phys. Rev. B **72**(18), 184415 (2005).
[106] J. Kübler, Theory of Itinerant Electron Magnetism (Clarendon, Oxford, 2000).
[107] J. Kübler, Phys. Rev. B **67**, 220403 (2003).
[108] J. Kübler, J. Phys.: Condens. Matter **18**, 9795 (2006).
[109] J. Kübler, G. H. Fecher, and C. Felser, Phys. Rev. B **76**, 024414 (2007).
[110] B. Alling, A. V. Ruban, and I. A. Abrikosov, Phys. Rev. B **79**, 134417 (2009).
[111] B. Hallstedt, D. Djurovic, J. von Appen, R. Dronskowski, A. Dick, F. Körmann, T. Hickel, and J. Neugebauer, Calphad **34**, 129 (2010).
[112] P. Gustafson, Scand. J. Metallurgy **14**(5), 259–267 (1985).
[113] F. Bloch, Z. Phys. **61**, 206 (1930).
[114] R. Kubo, Phys. Rev. **87**, 568 (1952).
[115] O. Källbäck, S. G. Humble, and G. Malmström, Phys. Rev. B **24**, 5214–5221 (1981).
[116] B. Stroka, J. Wosnitza, E. Scheer, H. Löhneysen, W. Park, and K. Fischer, Z. Phys. B, Condens. Matter **89**(1), 39–43 (1992).

[117] S. N. Kaul and M. S. Rao, J. Phys.: Condens. Matter **6**(36), 7403 (1994).
[118] M. Marinelli, F. Mercuri, S. Foglietta, and D. P. Belanger, Phys. Rev. B **54**, 4087–4092 (1996).
[119] M. Campostrini, M. Hasenbusch, A. Pelissetto, P. Rossi, and E. Vicari, Phys. Rev. B **65**, 144520 (2002).
[120] H. E. Stanley, Introduction to Phase Transitions and Critical Phenomena (Oxford University Press, Oxford, 1987).
[121] M. D. Kuz'min and A. M. Tishin, Europhys. Lett. **73**(3), 396 (2006).
[122] V. Franco, J. Blazquez, B. Ingale, and A. Conde, Annu. Rev. Mater. Res. **42**, 305–42 (2012).
[123] A. Arrott and J. Noakes, Phys. Rev. Lett. **19**, 786–89 (1967).
[124] M. D. Kuz'min, Phys. Rev. B **77**, 184431 (2008).
[125] M. D. Kuz'min, Phys. Rev. Lett. **94**, 107204 (2005).
[126] M. D. Kuz'min, M. Richter, and A. N. Yaresko, Phys. Rev. B **73**, 100401 (2006).
[127] L. D. Landau, Phys. Z. Sowjetunion **11**, 26 (1937).
[128] W. L. Bragg and E. J. Williams, Proc. R. Soc. Lond. A, Math. Phys. Sci. **145**(855), 699–730 (1934).
[129] W. L. Bragg and E. J. Williams, Proc. R. Soc. Lond. A, Math. Phys. Sci. **151**(874), 540–566 (1935).
[130] E. J. Williams, Proc. R. Soc. Lond. A, Math. Phys. Sci. **152**(875), 231–252 (1935).
[131] W. Gorsky, Z. Phys. **50**(1–2), 64–81 (1928).
[132] W. Shockley, J. Chem. Phys. **6**(3), 130–144 (1938).
[133] I. Ansara, B. Sundman, and P. Willemin, Acta Metall. **36**(4), 977–982 (1988).
[134] J. Lacaze and B. Sundman, Metall. Trans. A **22**(10), 2211–2223 (1991).
[135] N. Dupin and B. Sundman, Scand. J. Metallurgy **30**(3), 184–192 (2001).
[136] R. Kikuchi, Phys. Rev. **81**, 988 (1951).
[137] R. Kikuchi and S. G. Brush, J. Chem. Phys. **47**, 195 (1967).
[138] J. A. Barker, Proc. R. Soc. **A216**, 45 (1953).
[139] J. Hijmans and J. De Boer, Physica **21**, 471 (1955).
[140] T. Morita, J. Phys. Soc. Jpn. **12**, 753 (1957).
[141] T. Morita, J. Math. Phys. **13**, 115 (1972).
[142] R. Kikuchi and J. Murray, Calphad **9**(4), 311–348 (1985).
[143] C. G. Schön and G. Inden, Comput. Mater. Sci. **20**(1), 98–106 (2001).
[144] J. W. D. Connolly and A. R. Williams, Phys. Rev. B **27**, 5169 (1983).
[145] J. M. Sanchez, F. Ducastelle, and D. Gratias, Physica A **128**, 334 (1984).
[146] T. Mohri, J. Sanchez, and D. De Fontaine, Acta Metall. **33**(7), 1171–1185 (1985).
[147] A. Kusoffsky, N. Dupin, and B. Sundman, Calphad **25**(4), 549–565 (2001).
[148] B. Sundman, S. G. Fries, and W. Oates, Calphad **22**(3), 335–354 (1998).
[149] B. Sundman, I. Ohnuma, N. Dupin, U. R. Kattner, and S. G. Fries, Acta Mater. **57**(10), 2896–2908 (2009).
[150] R. Castanet and A. Ferrier, Compt. Rend. **15**, 272C (1971).
[151] I. Ohnuma, H. Enoki, O. Ikeda, R. Kainuma, H. Ohtani, B. Sundman, and K. Ishida, Acta Mater. **50**, 379 (2002).
[152] I. Ohnuma, S. Abe, S. Shimenouchi, T. Omori, R. Kainuma, and K. Ishida, ISIJ Int. **52**(4), 540–548 (2012).
[153] M. Cadeville and J. Moran-Lopez, Phys. Rep. **153**(6), 33–399 (1987).
[154] A. Berkowitz and E. Kneller, Magnetism and Metallurgy (Academic Press Inc., New York, 1969).
[155] J. B. Staunton, D. D. Johnson, and B. L. Gyorffy, J. Appl. Phys. **61**(8), 3693–3696 (1987).
[156] A. J. Pindor, J. Staunton, G. M. Stocks, and H. Winter, J. Phys. F, Met. Phys. **13**(5), 979 (1983).
[157] A. V. Ruban, S. Shallcross, S. Simak, and H. L. Skriver, Phys. Rev. B **70**(12), 125115 (2004).
[158] M. Rahaman, A. Ruban, A. Mookerjee, and B. Johansson, Phys. Rev. B **83**(5), 054202 (2011).
[159] M. Ekholm, H. Zapolsky, A. Ruban, I. Vernyhora, D. Ledue, and I. Abrikosov, Phys. Rev. Lett. **105**(16), 167208 (2010).
[160] J. M. Sanchez, M. C. Cadeville, V. Pierron-Bohnes, and G. Inden, Phys. Rev. B **54**, 8958 (1996).
[161] J. I. Seki, M. Hagiwara, and T. Suzuki, J. Mater. Sci. **14**, 2404 (1979).
[162] Y. Kakehashi, J. Magn. Magn. Mater. **54–57**, 1096 (1986).
[163] M. V. Nevitt, J. Appl. Phys. **31**, 155 (1960).
[164] I. Mirebeau, G. Parette, and J. W. Cable, J. Phys. F, Met. Phys. **17**, 191 (1987).
[165] D. D. Johnson, F. J. Pinski, and J. B. Staunton, J. Appl. Phys. **61**, 3715 (1987).
[166] J. C. Krause, J. Schaff, M. I. Costa, and C. Paduani, Phys. Rev. B **61**, 6196 (2000).
[167] J. A. Muñoz, M. S. Lucas, O. Delaire, M. L. Winterrose, L. Mauger, C. W. Li, A. O. Sheets, M. B. Stone, D. L. Abernathy, Y. Xiao, P. Chow, and B. Fultz, Phys. Rev. Lett. **107**, 115501 (2011).
[168] R. G. Jordan, X. Wang, A. M. Begley, S. L. Qiu, and Y. Liu, Solid State Commun. **78**, 1045 (1991).
[169] V. L. Moruzzi and P. M. Marcus, Phys. Rev. B **45**, 2934 (1992).
[170] M. S. Lucas, J. A. Muñoz, O. Delaire, N. Markovskiy, M. B. Stone, D. Abernathy, I. Halevy, L. Mauger, B. Keith, M. L. Winterrose, Y. Xiao, M. Lerche, and B. Fultz, Phys. Rev. B **82**, 144306 (2010).
[171] J. O. Andersson, Calphad **7**, 305 (1983).
[172] R. Wakelin and E. Yates, Proc. Phys. Soc. Lond. B **66**, 221 (1953).
[173] I. Ohnuma, O. Ikeda, R. Kainuma, B. Sundman, and K. Ishida, Z. Metallkd. **89**, 847 (1998).
[174] I. Ohnuma, R. Kainuma, and K. Ishida, in: CALPHAD and Alloy Thermodynamics, Proc. of a Symposium held at the 2002 TMS Annual Meeting, Seattle, WA, February 2002 (TMS, Warrendale, PA, 2002), pp. 61–78.
[175] I. Ohnuma et al., Paper presented at the CALPHAD XXVII, Beijing, China, May 18, 1998.
[176] O. Ikeda, I. Ohnuma, R. Kainuma, and K. Ishida, Intermetallics **9**, 755 (2001).
[177] L. Kaufman, E. V. Clougherty, and R. J. Weiss, Acta Metall. **11**, 323 (1963).
[178] H. Hasegawa and D. G. Pettifor, Phys. Rev. Lett. **50**, 130–133 (1983).
[179] I. Leonov, A. I. Poteryaev, V. I. Anisimov, and D. Vollhardt, Phys. Rev. Lett. **106**, 106405 (2011).
[180] J. Zarestky and C. Stassis, Phys. Rev. B **35**, 4500–4502 (1987).
[181] H. C. Hsueh, J. Crain, G. Y. Guo, H. Y. Chen, C. C. Lee, K. P. Chang, and H. L. Shih, Phys. Rev. B **66**, 052420 (2002).
[182] F. Körmann, Magnetic systems studied by first-principles thermodynamics, Ph.D. thesis, University of Paderborn

(2011), http://digital.ub.uni-paderborn.de/hs/download/pdf/8865.
[183] H. Hasegawa, M. W. Finnis, and D. G. Pettifor, J. Phys. F, Met. Phys. **17**(10), 2049 (1987).
[184] I. Leonov, A. I. Poteryaev, V. I. Anisimov, and D. Vollhardt, Phys. Rev. B **85**, 020401 (2012).
[185] A. V. Ruban and V. I. Razumovskiy, Phys. Rev. B **85**, 174407 (2012).
[186] F. Körmann, A. Dick, B. Grabowski, T. Hickel, and J. Neugebauer, Phys. Rev. B **85**, 125104 (2012).
[187] D. Dever, J. Appl. Phys. **43**(8), 3293–3301 (1972).
[188] S. L. Dudarev, R. Bullough, and P. M. Derlet, Phys. Rev. Lett. **100**, 135503 (2008).
[189] Z. Yao, M. L. Jenkins, M. Hernandez-Mayoral, and M. A. Kirk, Philos. Mag. **90**(35–36), 4623–4634 (2010).
[190] E. Martinez, O. Senninger, C. C. Fu, and F. Soisson, Phys. Rev. B **86**, 224109 (2012).
[191] M. Y. Lavrentiev, K. Mergia, M. Gjoka, D. Nguyen-Manh, G. Apostolopoulos, and S. L. Dudarev, J. Phys.: Condens. Matter **24**(32), 326001 (2012).
[192] M. Y. Lavrentiev, S. L. Dudarev, and D. Nguyen-Manh, J. Appl. Phys. **109**(7), 07E123 (2011).

